NASA TECHNICAL MEMORANDUM

CLASSIFICATION CHANGED
UNCLASSIFIED
TO.....................

By Authority of .... Date ....

BLOW-IN-DOOR EJECTOR NOZZLE PERFORMANCE COMPARISON BETWEEN FIXED-OPEN AND FREE-FLOATING DOOR CONFIGURATIONS

CLASSIFICATION CHANGED
UNCLASSIFIED
TO.....................

By Authority of TD 71-36 Date 12-15-70

by Rodney F. Lauer, Jr., and Charles E. Mercer

Langley Research Center

Langley Station, Hampton, Va.

BLOW-IN-DOOR EJECTOR NOZZLE PERFORMANCE COMPARISON

BETWEEN FIXED-OPEN AND FREE-FLOATING DOOR CONFIGURATIONS

By Rodney F. Lauer, Jr., and Charles E. Mercer

Langley Research Center
Langley Station, Hampton, Va.

NATIONAL AERONAUTICS AND SPACE ADMINISTRATION

BLOW-IN-DOOR EJECTOR NOZZLE PERFORMANCE COMPARISON
BETWEEN FIXED-OPEN AND FREE-FLOATING DOOR CONFIGURATIONS*

By Rodney F. Lauer, Jr., and Charles E. Mercer
Langley Research Center

SUMMARY

An investigation of the effect on nozzle performance of simulating free-floating blow-in-door ejector nozzles with fixed open-door configurations, and of blocking one-third of the blow-in-doors closed, as might be required for fuselage installation in an airplane, has been conducted in the Langley 16-foot transonic tunnel. Fixed-open and free-floating blow-in-door ejector nozzles with a conical shroud and a curved shroud (a partial ogive) were tested with primary nozzle-exit areas representing a military power setting for subsonic speeds and a partial afterburning power setting for low supersonic speeds. The conical shroud was used for that part of the investigation concerned with door-blockage effects. A hydrogen peroxide gas generator provided hot primary exhaust gases through a range of total-pressure ratios from 1.2 to 4.6, depending on Mach number; a high pressure air system provided secondary air at corrected weight-flow ratios up to 0.08.

The results indicate that a loss in nozzle performance is incurred by simulating blow-in-door ejector nozzles with fixed open-door configurations. The effect on thrust-minus-drag performance is strongly influenced by secondary airflow, and while significant effects are noticed with the curved shroud configuration without secondary airflow, these effects are absent in the conical shroud configurations. If possible, blow-in-door ejector nozzle performance comparisons should be made using data obtained from free-floating blow-in-door nozzles. Blocking closed one-third of the floating blow-in-doors results in slight performance losses at supersonic speeds and in mixed effects at subsonic speeds, depending on Mach number, primary total-pressure ratio, and corrected secondary weight-flow ratio.

INTRODUCTION

The principles of operation and the performance characteristics of various blow-in-door ejector nozzles have been published in references 1 to 5. The data in references 3,

---

*Title, Unclassified.

4, and 5 were obtained with the doors fixed in the full-open position. For the speed range and operating conditions of these investigations, it was predicted that the doors would be in the full-open position if free-floating doors had been used; however, as pointed out in reference 3, pressure data on the doors indicated that the doors may tend to float to some position other than full open. Because partial closing of the doors could affect the nozzle performance, the present investigation was undertaken to evaluate the effect on nozzle performance of simulating the free-floating doors with fixed-open doors. In addition, the effect of blow-in-door blockage (as might occur in fuselage installation in an airplane) was studied by fixing two 60° segments of the blow-in-doors closed around the periphery of the nozzle of one free-floating door configuration.

The tests were conducted on an isolated nacelle model. Both the free-floating and fixed doors were investigated with two shroud configurations, the external shape of one being conical and the other being curved (a partial ogive). The blockage effects were determined on the conical shroud configuration.

Force and pressure data were obtained from static tests and at Mach numbers ranging from 0.50 to 0.90 and from 1.15 to 1.25 at an angle of attack of 0°. The ratio of primary-jet total pressure to free-stream static pressure varied from 1.2 to 4.6, depending on Mach number; the corrected ratios of secondary air weight flow to primary weight flow varied from 0 to about 0.08. Hot primary exhaust gases were provided by a hydrogen peroxide gas generator and unheated secondary air by a high pressure air system.

SYMBOLS

Measurements for this investigation were taken in U.S. Customary Units. Equivalent values are indicated parenthetically in the International System (SI).

A   cross-sectional area, sq in. (m^2)

C_f external skin-friction drag coefficient, $\dfrac{\text{Skin friction}}{q_\infty A_{max}}$

d   diameter, in. (m)

F_{bal} axial force measured on balance (positive as thrust), lbf (N)

$F_{e - D}$ ejector gross thrust minus drag, lbf (N)

$F_{i,p}$ ideal jet thrust for complete isentropic expansion of measured primary weight

$$\text{flow,} \quad m_p \sqrt{2R_p \frac{\gamma_p}{\gamma_p - 1} T_{t,p} \left[1 - \left(\frac{p_\infty}{p_{t,p}} \right)^{\frac{\gamma_p - 1}{\gamma_p}} \right]}, \text{ lbf (N)}$$

F_p primary-nozzle gross thrust, lbf (N)

f_i calculated skin-friction drag force on internal surface of afterbody due to secondary airflow, lbf (N)

g gravitational acceleration, ft/sec^2 (m/s^2)

M free-stream Mach number

m measured mass-flow rate, slugs/s (kg/s)

p static pressure, lbf/in^2 (N/m^2)

q dynamic pressure, lbf/in^2 (N/m^2)

R gas constant, $\dfrac{\text{ft-lbf}}{\text{slug-}^\circ\text{R}}$ $\left(\dfrac{\text{J}}{\text{kg-}^\circ\text{K}} \right)$ R_p = 2250.6 (376.7); R_s = 1716.3 (287.3)

T temperature, $^\circ$R ($^\circ$K)

V_s velocity of secondary airstream at model station 36.87 in. (93.65 cm), ft/sec (m/s)

w measured weight-flow rate, lbf/sec (No equivalent SI unit)

$w_{i,p}$ ideal primary weight-flow rate,

$$p_{t,p} A_p \left(\frac{p_p}{p_{t,p}} \right)^{\frac{1}{\gamma_p}} \sqrt{\frac{2}{R_p T_{t,p}} \frac{\gamma_p}{\gamma_p - 1} \left[1 - \left(\frac{p_p}{p_{t,p}} \right)^{\frac{\gamma_p - 1}{\gamma_p}} \right]}, \text{ lbf/sec (No equivalent SI unit)}$$

x longitudinal distance from model station 47.74 in. (121.26 cm), positive rearward, in. (m)

γ ratio of specific heats $\left(\gamma_p = 1.267; \quad \gamma_s = 1.400 \right)$

$\Delta\left(\dfrac{F_e - D}{F_{i,p}}\right)$ incremental gross ejector thrust-minus-drag ratio (free-floating blow-in-door performance minus fixed-open blow-in-door performance)

θ meridian angle, deg (see fig. 3)

μ ratio of gas constants, $\dfrac{R_p}{R_s} = 1.31$

τ total-temperature ratio, $\dfrac{T_{t,s}}{T_{t,p}}$

ω ratio of secondary airflow rate to primary flow rate, $\dfrac{w_s}{w_p}$

$\omega\sqrt{\dfrac{\tau}{\mu}}$ corrected secondary air weight-flow ratio

Subscripts:

a   ambient

b   maximum diameter of tailpipe (see figs. 1 and 3)

cyl   cylindrical portion of afterbody

e   cavity between flexible seal and external surface (see fig. 1)

i   secondary air passage

max   maximum

N   external convergent surface of primary nozzle

p   primary-jet exit

s   secondary air

seal   seal station (see fig. 1)

t   total or stagnation conditions

w   maximum internal diameter of afterbody (see fig. 3)

∞   free-stream conditions

A bar over a symbol denotes an average value.

APPARATUS AND PROCEDURE

Model

A sketch of the strut-supported jet-engine simulator and afterbody used in this investigation is shown in figure 1; a photograph of a model installed in the test section of the Langley 16-foot transonic tunnel is given in figure 2(a), and afterbody configurations are shown in figure 2(b). The model was supported by a sweptback strut attached to a sting having a constant cross-sectional area downstream from the point of intersection with the trailing edge of the strut. The model center line was 3.343 model diameters above the test-section center line.

The model consisted of an ogival forebody, a cylindrical centerbody with a maximum diameter of 6 in. (15.24 cm), and an afterbody which was composed of a cylindrical section from model station 36.87 in. (93.65 cm) to 48.48 in. (123.14 cm), a boattail to station 53.93 in. (136.98 cm), blow-in-doors to station 56.24 in. (142.85 cm), and the ejector shroud. Unheated secondary air supplied by a high-pressure air system was piped into the forward section of the model and channeled to the ejector. Hot primary exhaust gases were supplied by a hydrogen peroxide gas generator similar to the one described in reference 6. The gas generator was attached to the support system, whereas the afterbody was attached to the balance.

The ejector-nozzle configurations investigated are referred to by a code consisting of one letter and two digits. The letter denotes the primary-nozzle size: M for military power settings $\left(A_p/A_{max} = 0.228\right)$ used for subsonic flight; and A for partial afterburning $\left(A_p/A_{max} = 0.273\right)$ used for transonic flight. These area ratios were selected as being typical of a high-performance airplane-engine combination. The first digit denotes the boattail—blow-in-door combination: The number 1 indicates the blow-in-doors fixed in the full-open position, 2 indicates the free-floating, pressure-actuated blow-in-doors, and 3 indicates the free-floating, pressure-actuated blow-in-doors with two of the six door segments blocked in the closed position. All configurations have the same boattail contours ahead of the blow-in-doors. The second digit denotes the ejector shroud: Shroud 1 has conical external contours, while shroud 3 is a section of an ogive. The leading- and trailing-edge diameters of shroud 3 are less than those of shroud 1, and shroud 3 is slightly shorter. The internal contours of the two shrouds are different,

shroud 3 having the smaller minimum cross-sectional area. (See fig. 3 for configuration details.)

Instrumentation

As in reference 5, static-pressure orifices were located along the primary-nozzle external surface and at both the internal and external seal stations around the nacelle. The total temperature and total pressure of the primary gas stream was measured upstream of the primary-nozzle throat, and similar measurements for the secondary airstream were made in the secondary air passage. The axial force on the afterbody was measured by means of a strain-gage balance. (See fig. 1.) Electronic flowmeters were used to measure the hydrogen peroxide flow rate to the primary nozzle; the secondary airflow rate was determined using a venturi installed in the high-pressure air supply line.

Tests

Data were obtained from static tests and at Mach numbers from 0.50 to 0.90 and from 1.15 to 1.25 at 0° angle of attack. Depending on Mach number, the ratio of primary-jet total pressure to free-stream static pressure $p_{t,p}/p_\infty$ was varied from 1.2 to 4.6, and the corrected secondary air weight-flow ratio $\omega\sqrt{\frac{\tau}{\mu}}$ was varied from 0 to 0.08. The general procedure was to set first a nominal value of the ratio $p_{t,p}/p_\infty$ and then to record data at several values of secondary airflow from 0 to the maximum value for each Mach number. The procedure was repeated for several ascending values of $p_{t,p}/p_\infty$ through the desired range. Numerous cycles were rerun for decreasing values of $p_{t,p}/p_\infty$, although to reduce testing time no attempt was made to repeat exact settings of the ratio $p_{t,p}/p_\infty$.

The thrust of the primary nozzle F_p was obtained as a function of total-pressure ratio at static conditions. The calibration curves shown in figure 4 were then used to determine the values of F_p in the wind-tunnel tests.

The Reynolds number based on model length for the tests was approximately 18.5×10^6. Boundary-layer transition was fixed by a strip of carborundum grains near the model nose.

Data Reduction

Model data recorded on magnetic tape were used to compute standard force and pressure coefficients. Pressure drag on the primary-nozzle external surface was obtained by assigning to each pressure orifice an incremental area projected on a plane normal to the model axis and numerically integrating the incremental forces. No

correction was made for strut interference since the data in reference 7 indicate that the effect is small for this support system.

The overall thrust minus drag of the ejector was computed from the following equation:

$$F_e - D = F_p + \int_{A_p}^{A_b} \left(p_N - p_\infty\right)dA + F_{bal} + \left(\bar{p}_i - p_\infty\right)\left(A_{seal} - A_w\right) + \left(\bar{p}_e - p_\infty\right)\left(A_{max} - A_{seal}\right)$$

$$+ \frac{w_s V_s}{g} + \left(\bar{p}_i - p_\infty\right)\left(A_w - A_b\right) + C_{f,cyl}q_\infty A_{max} + f_i$$

The balance axial-force term F_{bal} includes the external skin-friction drag for the entire afterbody, the external pressure drag for the boattail, blow-in-doors, and shroud, the friction and pressure forces on the internal surfaces of the afterbody due to secondary airflow, and all forces on both the convergent and divergent internal surfaces of the ejector shroud. Skin-friction calculations were based on an equivalent wetted area of a flat plate and on an average Reynolds number.

RESULTS AND DISCUSSION

Data Presentation

The basic data are presented in figures 5 and 6, in which the variations of ejector pressure ratio (ejector pumping characteristics) and thrust-minus-drag ratio with corrected secondary weight-flow ratio are shown at specified values of Mach number and nominal values of primary-jet total-pressure ratio. Cross plots of these data then permit presentation of the performance characteristics as functions of primary-jet total-pressure ratio at constant values of corrected secondary air weight-flow ratio of 0, 0.03, and 0.05, as shown in figures 7 and 8. In this form the effects on performance of changes in configuration geometry and changes in operating conditions become more readily apparent.

Comparative Performance

Because the present investigation pertains to exhaust nozzles intended for application to a mixed-flow afterburning turbofan engine, comparisons of performance are made at values of the primary-jet total-pressure ratio appropriate to that engine type. A typical variation of primary-jet total-pressure ratio with Mach number for a turbofan engine is presented in figure 9. The variation with Mach number of the performance of the fixed-open, free-floating, and partially blocked blow-in-door configurations for three constant values of corrected secondary flow is presented in figure 10 for conditions

corresponding to the jet total-pressure ratio schedule of figure 9. Similar comparisons at other values of primary-jet total-pressure ratio may be obtained by cross-plotting the performance data of figure 8.

Effect of simulating blow-in-door ejector nozzles with fixed-open door configurations.- The comparative performance data presented in figure 10(a) for the conical shroud configurations indicate that without secondary airflow there are only slight effects (less than 1 percent) due to simulating blow-in-door ejector nozzles with fixed-geometry configurations. As secondary airflow is increased, however, the thrust-minus-drag ratio of the free-floating door configurations (M-21 and A-21) increases more rapidly than that of the fixed-door configurations (M-11 and A-11). The incremental gross ejector thrust-minus-drag ratio (free-floating blow-in-door performance minus fixed-open blow-in-door performance) is presented in figure 11 as a function of corrected secondary weight-flow ratio. For all Mach numbers the value of $\Delta\left(\dfrac{F_e - D}{F_{i,p}}\right)$ increases as secondary airflow is increased. At $M = 1.20$ for $\omega\sqrt{\dfrac{\tau}{\mu}} = 0.05$ the loss in performance due to simulating the blow-in-door ejector nozzle with a fixed-geometry configuration is 0.014.

This loss in performance is not surprising. As indicated in reference 3, at some Mach numbers and pressure ratios, and in the present investigation at some values of secondary airflow, conditions might tend to move the blow-in-doors away from the full-open position. Apparently these conditions existed for the conical shroud configurations with the addition of secondary airflow. As a result, for the fixed-open blow-in-door configurations, airflow in the vicinity of the blow-in-door inlet and shroud was adversely affected and consequently there was a loss in performance.

A similar effect is noted for the curved shroud configuration, though the data in figure 10(b) show that there is an effect even without secondary airflow. For this shroud shape, with no secondary airflow, Mach number and pressure-ratio conditions are apparently sufficient to move the blow-in-doors from the full-open position except at $M = 0.70$. Data in figure 11 show that the change in performance due to secondary airflow from $\omega\sqrt{\dfrac{\tau}{\mu}} = 0$ to $\omega\sqrt{\dfrac{\tau}{\mu}} = 0.05$ is about the same for both shroud configurations, but the level of the ratio $\Delta\left(\dfrac{F_e - D}{F_{i,p}}\right)$ of the curved shroud configuration is higher than that of the conical shroud configuration at all Mach numbers except $M = 0.70$. As previously stated, at $M = 1.20$ for $\omega\sqrt{\dfrac{\tau}{\mu}} = 0.05$ the loss in performance due to simulating the free-floating blow-in-door ejector nozzle with a fixed-geometry configuration is 0.014 if the conical shroud is used; the corresponding value for the curved shroud is 0.021. In general, while the fixed-open blow-in-door configurations give a good approximation of the blow-in-door ejector nozzle performance level over the range of conditions investigated,

they do not completely simulate the flow in a free-floating blow-in-door ejector nozzle. Although blow-in-door position was not measured, the data indicate that the blow-in-doors of both ejector nozzle shroud configurations tend to move away from the full-open position, especially during operation at the higher values of secondary airflow.

Effect of partially blocking blow-in-doors closed.- The effect on performance of blocking closed two 60° segments of the floating blow-in-doors around the periphery of the ejector is presented in figure 10(a). Door blockage causes only a slight loss (less than 1 percent) in performance at supersonic speeds for all values of secondary weight-flow ratio. This loss is small because the blow-in-doors probably tend to close at these pressure-ratio conditions and thus the geometric alteration of holding one-third of the blow-in-doors in the closed position does not significantly affect the gross ejector performance. A small loss would be expected, however, because of the asymmetry of the flow through the blow-in-door inlet into the ejector shroud.

The performance losses at $M = 0.70$ may also be caused by the asymmetrical flow of air through the blow-in-door inlet into the shroud. A comparison of figures 7(c) and 7(d) shows that the pressure in the secondary air passage is lower for the blocked door configuration than that for the free-floating door configuration. This pressure difference tends to verify the lower performance level for the blocked door configuration. The lower secondary air passage pressure is probably a result of the overexpansion of the primary exhaust products toward the blocked doors which consequently reduces the secondary passage pressure for a given secondary flow rate.

At $M = 0.50$ and at low jet total-pressure ratios, partially blocking the blow-in-doors closed increases the performance level. At higher pressure ratios, a loss in performance similar to that at $M = 0.70$ is noted. (See figs. 8(c) and 8(d).)

CONCLUSIONS

An investigation of the effects of simulating blow-in-door ejector nozzles with fixed open-door configurations and the effect of blocking one-third of the floating blow-in-doors closed has been conducted in the Langley 16-foot transonic tunnel. The effects of fixed-door simulation were studied at subsonic and low supersonic speeds with configurations having conical and curved shrouds. The effects of door blockage were examined with the conical shroud configuration over a similar speed range. The results of the investigation are as follows:

1. Blow-in-door ejector nozzle performance may be satisfactorily approximated, for the configurations and conditions investigated, with fixed-open blow-in-door configurations at zero secondary airflow. With the addition of secondary airflow, however, the approximation becomes less satisfactory. Increasing secondary airflow rates increases

free-floating blow-in-door nozzle performance more than fixed-open blow-in-door nozzle performance.

2. The change in performance due to simulating blow-in-door ejector nozzles with fixed geometry configurations is a function of Mach number, primary total-pressure ratio, corrected secondary weight-flow ratio, and shroud geometry.

3. Blocking one-third of the floating blow-in-doors closed around the nozzle periphery results in a slight loss in performance at supersonic speeds and in mixed effects at subsonic speeds, depending on Mach number, pressure ratio, and corrected secondary weight-flow ratio.

Langley Research Center,
    National Aeronautics and Space Administration,
        Langley Station, Hampton, Va., October 18, 1965.

REFERENCES

1. Anon.: Blow-In Door Exhaust Nozzle Summary. Inst. Memo Rept. 187, Pratt & Whitney Aircraft, Oct. 1961. (Revised Nov. 1961.)

2. Installation Engineering: JTF10A-20 Engine — Exhaust Nozzle and Ejector. Inst. Memo Rept. 189, Pratt & Whitney Aircraft, Nov. 1961.

3. Kirkham, Frank S.; and Schmeer, James W.: Performance Characteristics At Mach Numbers up to 1.29 of a Blow-In-Door Ejector Nozzle With Doors Fixed in Full-Open Position. NASA TM X-830, 1963.

4. Schmeer, James W.; Mercer, Charles E.; and Kirkham, Frank S.: Effect of Bypass Air on the Performance of a Blow-In-Door Ejector Nozzle at Transonic Speeds. NASA TM X-896, 1963.

5. Mercer, Charles E.; Schmeer, James W.; and Lauer, Rodney F., Jr.: Performance of Several Blow-In-Door Ejector Nozzles at Subsonic and Low-Supersonic Speeds. NASA TM X-1163, 1967.

6. Runckel, Jack F.; and Swihart, John M.: A Hydrogen Peroxide Hot-Jet Simulator for Wind-Tunnel Tests of Turbojet-Exit Models. NASA MEMO 1-10-59L, 1959.

7. Norton, Harry T., Jr.; Runckel, Jack F.; and Pendergraft, Odis C., Jr.: Transonic Performance of Two Convergent-Divergent Ejector Nozzles Designed for Corrected Secondary Flows of 3 and 9.4 Percent. NASA TM X-909, 1964.
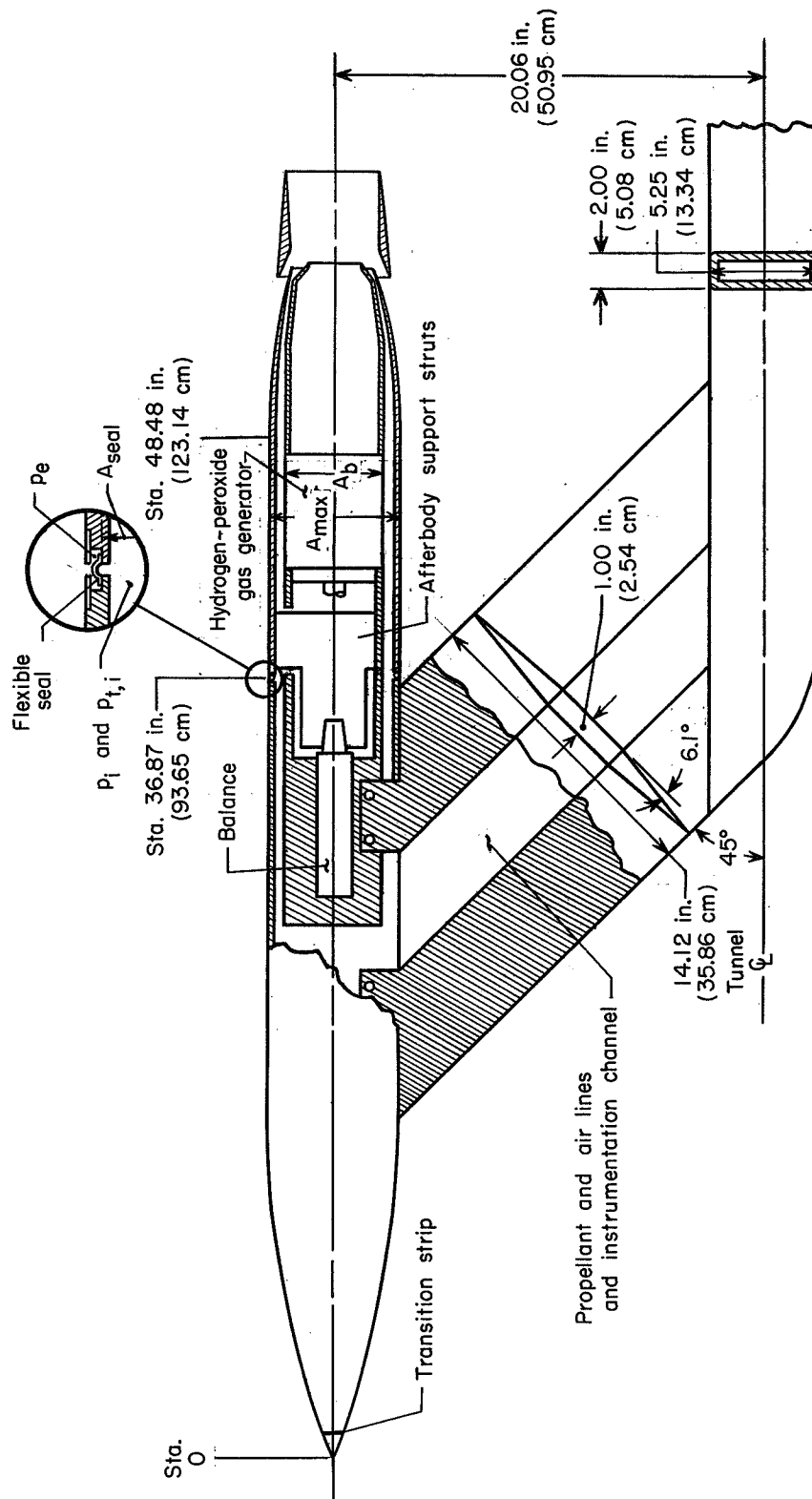
Figure 1.- Sketch of model installation.

11
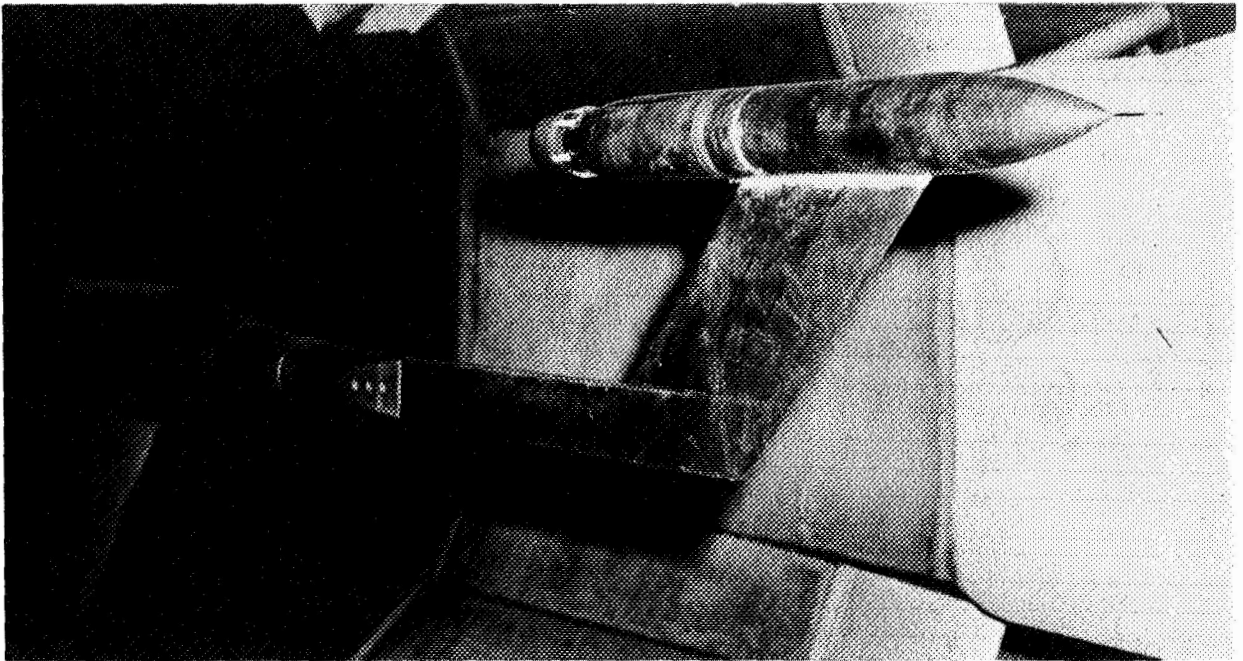
(a) Configuration M-11 mounted in the Langley 16-foot transonic tunnel. L-63-3773
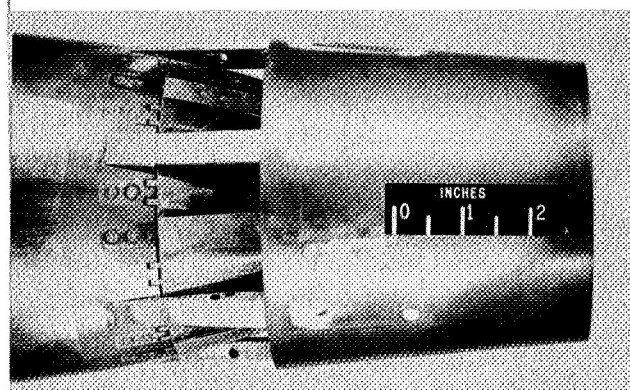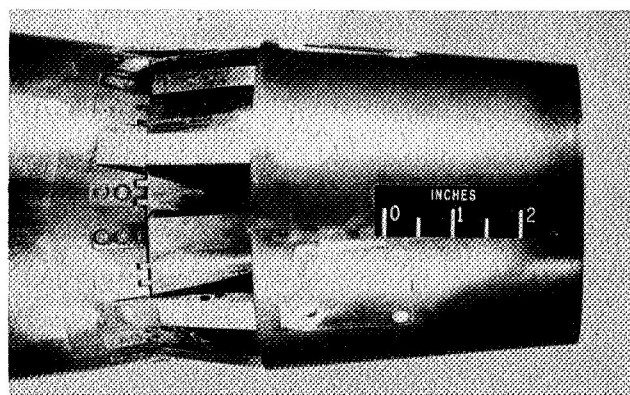
Figure 2.- Photographs of models.
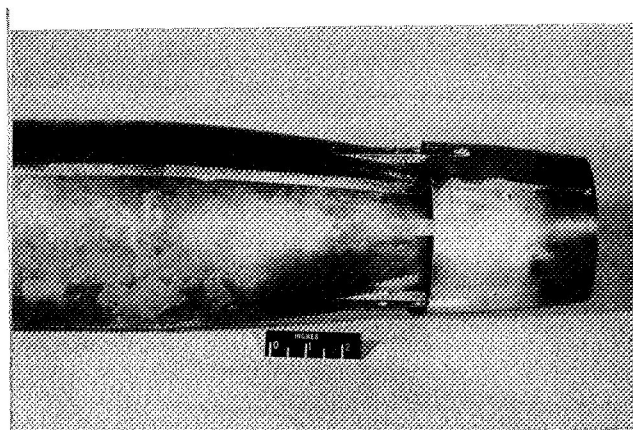
Configuration M-13   L-63-3619
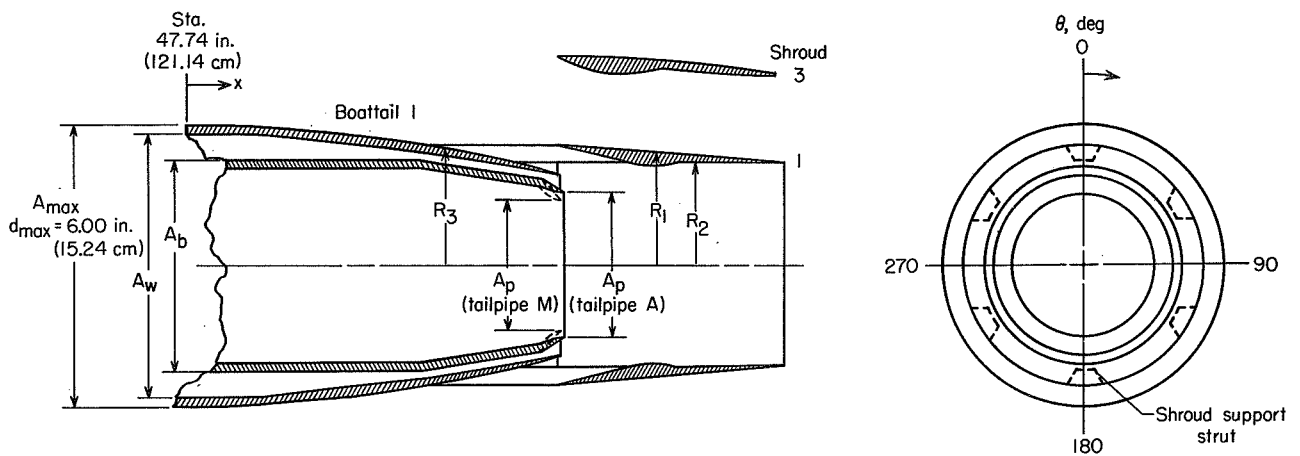

Configuration M-21   L-63-3620

Configuration M-31

(b) Ejector configurations.   L-63-3621
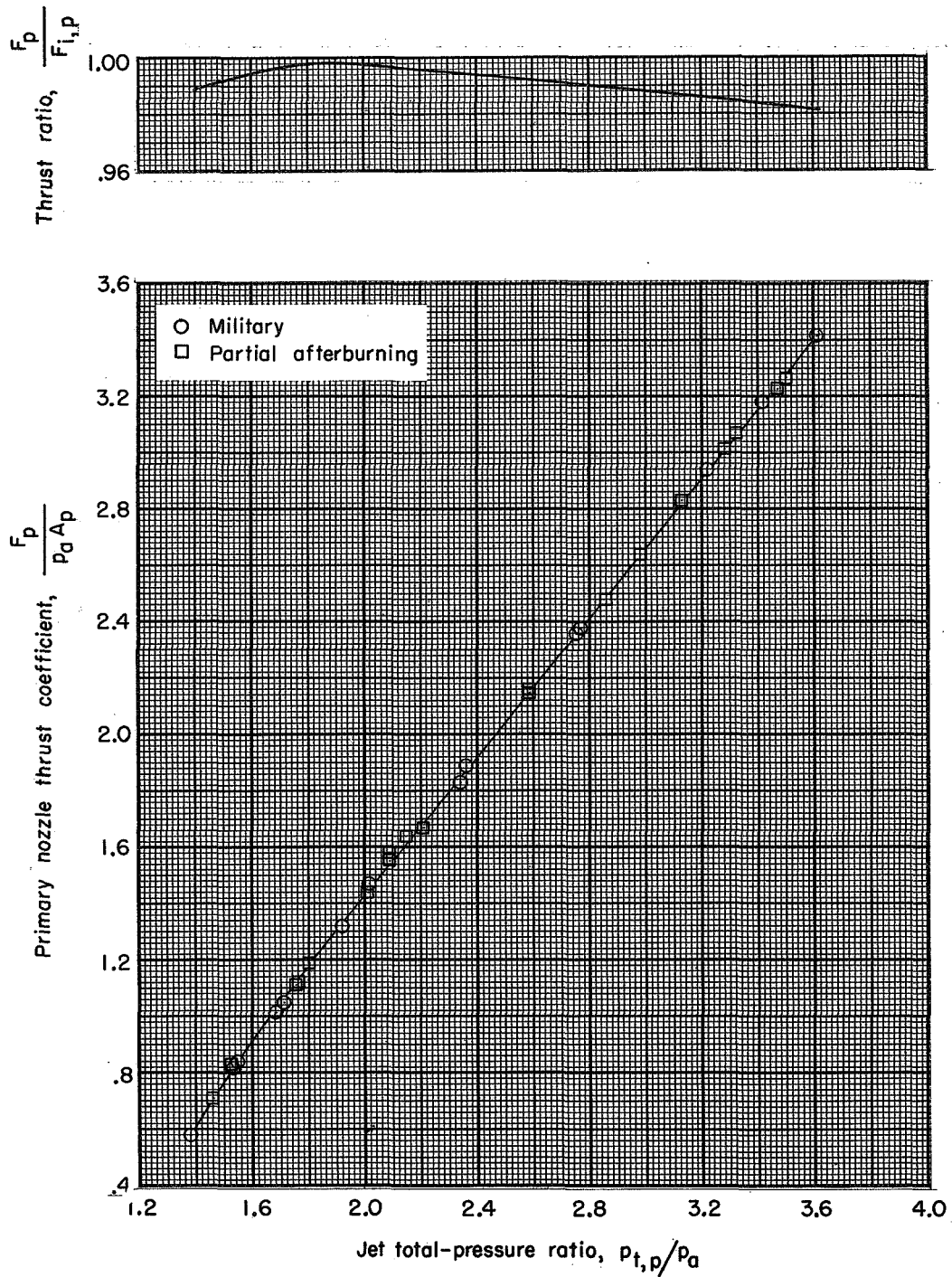
Figure 2.- Concluded.

13

Configuration M-11 and A-11						
Coordinates						
Shroud			Boattail		Tailpipe A	
x/d_{max}	R_1/d_{max}	R_2/d_{max}	x/d_{max}	R_3/d_{max}	x/d_{max}	d_p/d_{max}
1.4122	0.4300	0.4278	0	0.5000	1.4368	0.5230
		Straight line taper	.1230	.5000		
			.1950	.4958	**M**	
			.2668	.4923	x/d_{max}	d_p/d_{max}
1.6060		.3807	.3387	.4887	1.4213	0.4780
1.6283	Straight	.3748	.4105	.4852		
1.6507	line	.3703	.4823	.4807		
1.6728	taper	.3665	.5543	.4752		
1.6952		.3642	.6262	.4692		
1.7175		.3625	.6980	.4617		
1.7397		.3610	.7698	.4537		
1.7798		.3610	.8417	.4438		
1.8335		.3677	.9137	.4338		
2.2255	.3632	.3610	.9855	.4218		
			1.0325	.4132		
			1.0573	Straight line taper		
			1.1292			
			1.2010			
			1.2730	.3622		
			1.3448	.3457		
			1.4167	.3233		

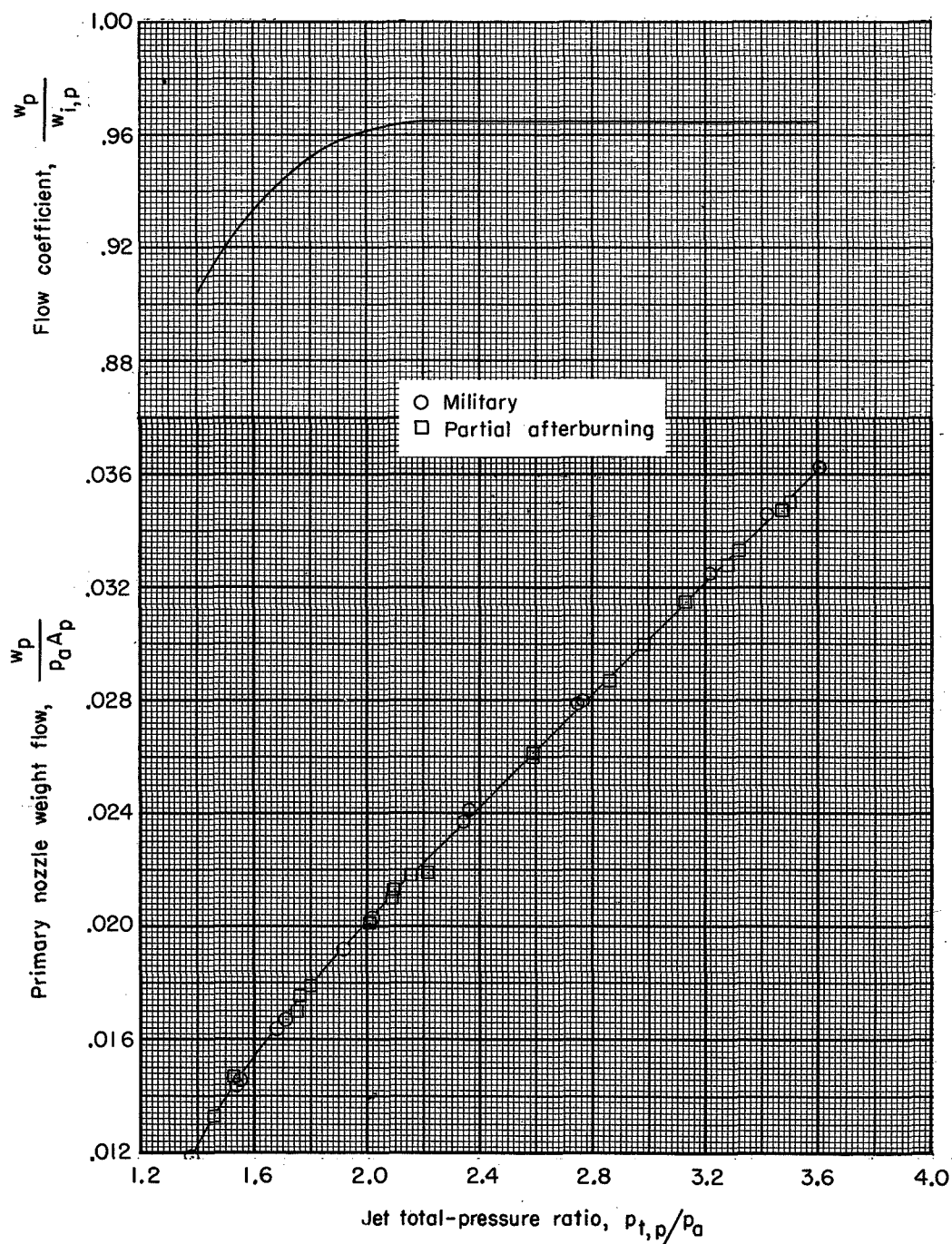| Configuration M-13 and A-13						
Coordinates						
Shroud			Boattail		Tailpipe A	
x/d_{max}	R_1/d_{max}	R_2/d_{max}	x/d_{max}	R_3/d_{max}	x/d_{max}	d_p/d_{max}
1.4167	0.4133	0.4115	0	0.5000	1.4368	0.5230
1.5058	.4125	.3813	.1230	.5000		
1.5282		.3738	.1950	.4958	**M**	
1.5503		.3670	.2668	.4923	x/d_{max}	d_p/d_{max}
1.5727		.3615	.3387	.4887	1.4213	0.4780
1.5950	.4098	.3578	.4105	.4852		
1.6172		.3562	.4823	.4807		
1.6395		.3558	.5543	.4752		
1.6618		.3565	.6262	.4692		
1.6840	.4058	.3575	.6980	.4617		
1.7063		.3588	.7698	.4537		
1.7287		.3608	.8417	.4438		
1.7510		.3632	.9137	.4338		
1.7732	.4005	.3662	.9855	.4218		
1.7955		.3690	1.0325	.4132		
1.8178		.3718	1.0573	Straight line taper		
1.8288		.3735	1.1292			
1.8623	.3935	.3710	1.2010			
1.9515	.3847	.3643	1.2730	.3622		
2.0407	.3738	.3572	1.3448	.3457		
2.1297	.3618	.3505	1.4167	.3233		
2.1520		.3490				
2.1743		.3478				
2.2057	.3497	.3478				

Notes: 1. Configurations M-21 and A-21 are identical to configurations M-11 and A-11, and configurations M-23 and A-23 are identical to M-13 and A-13 except that the blow-in-doors ($1.1375 < x/d_{max} < 1.4167$) are hinged at $x/d_{max} = 1.1375$ and the trailing edges are free to float radially from the open position to the shroud lip.

2. Configurations M-31 and A-31 are identical to configurations M-21 and A-21 except that the blow-in-doors are blocked in the closed position for $180° < \theta < 240°$ and $300° < \theta < 360°$.

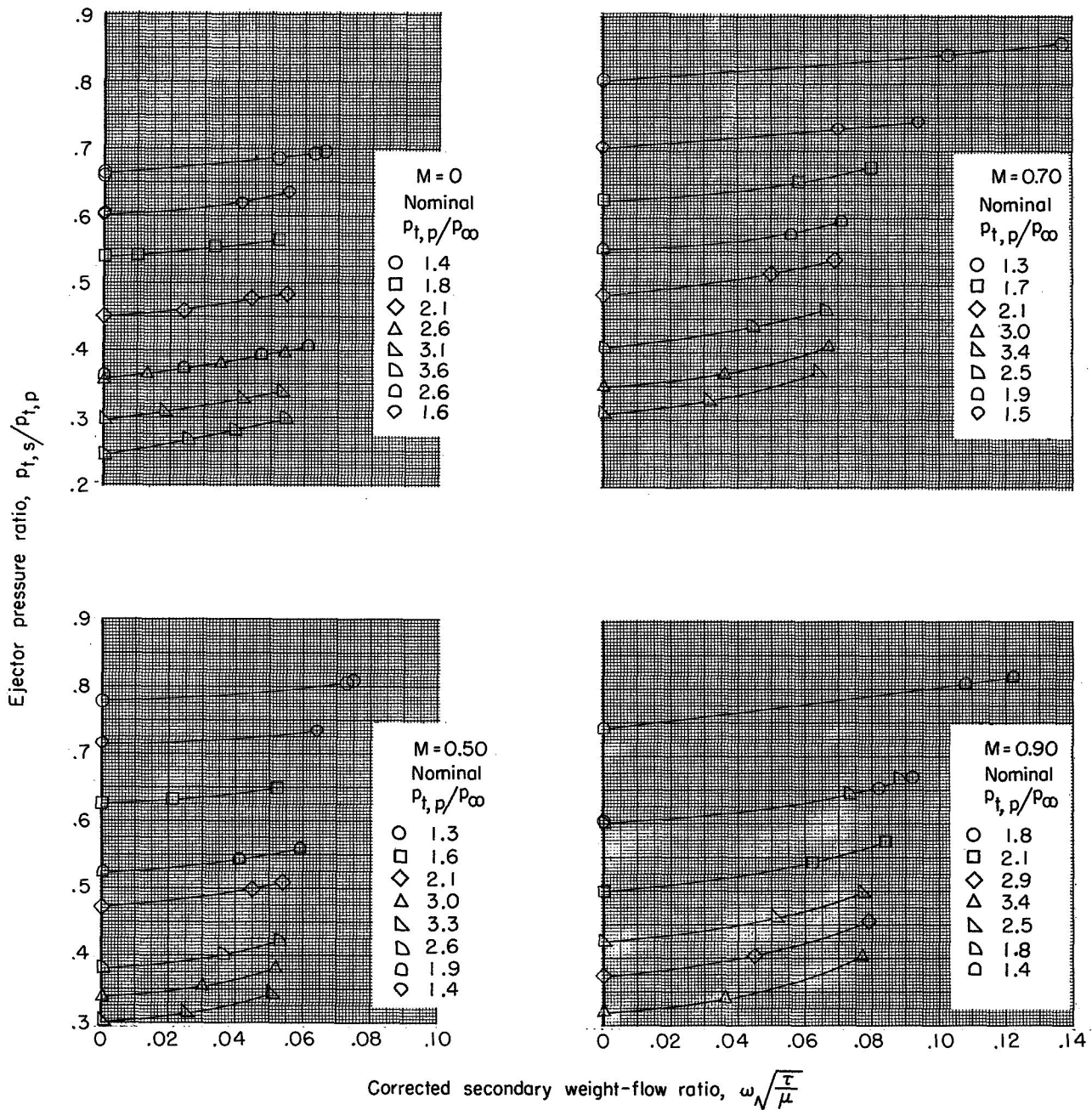Figure 3.- Details of blow-in-door ejector nozzle.

(a) Thrust performance.

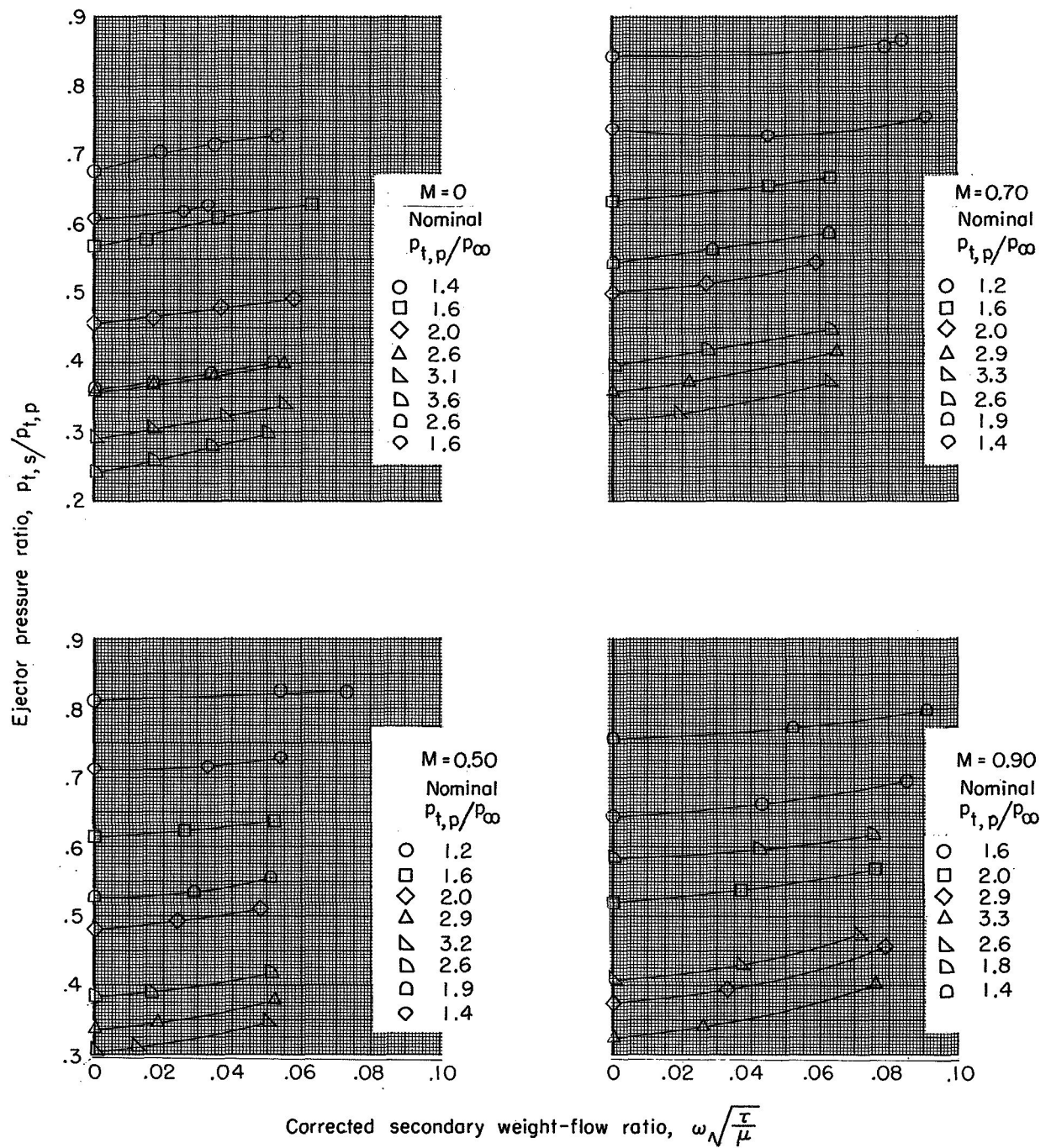Figure 4.- Performance of primary convergent nozzles in quiescent air.

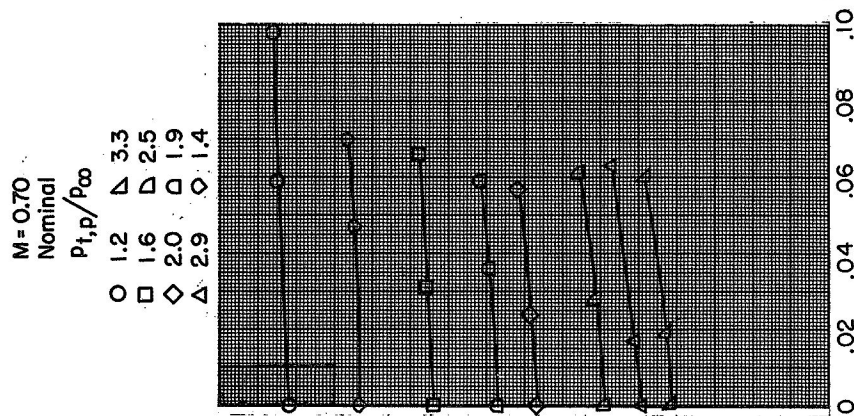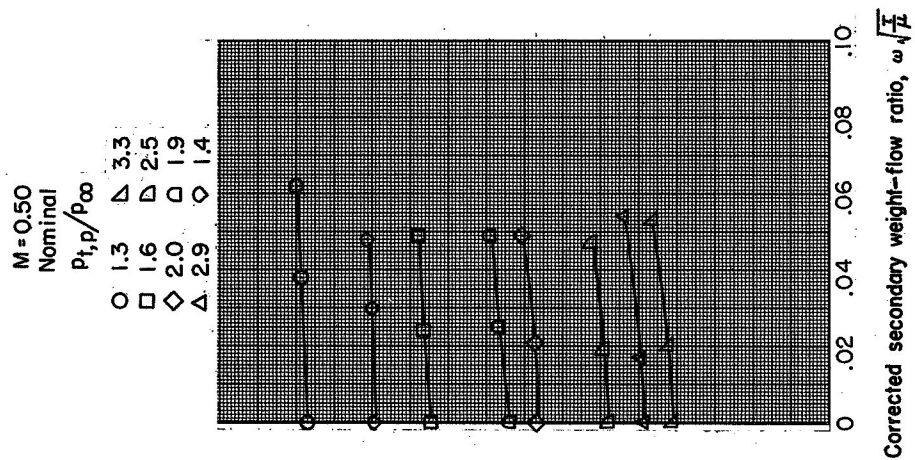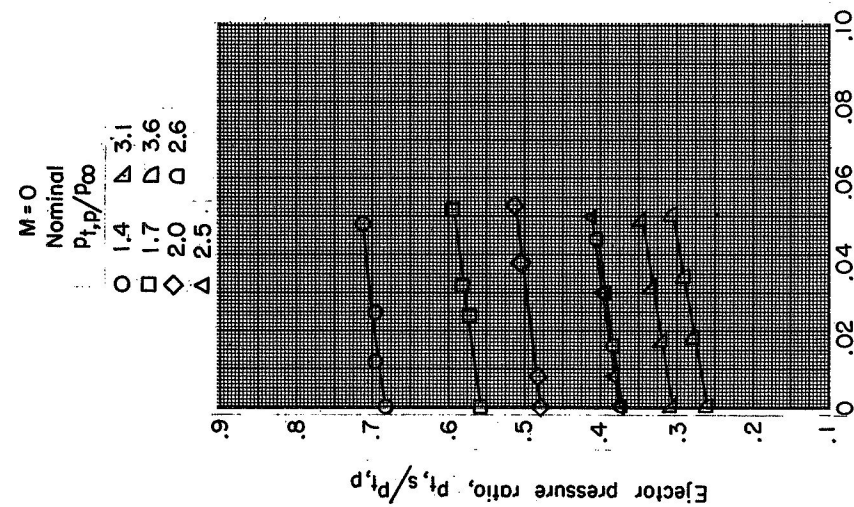(b) Flow performance.

Figure 4.- Concluded.

(a) Configuration M-11.

Figure 5.-   Variation of ejector pressure ratio with corrected secondary weight-flow ratio for various primary-jet total-pressure ratios and Mach numbers.

M = 0

	Nominal $p_{t,p}/p_\infty$
O	1.4
□	1.6
◇	2.0
△	2.6
◁	3.1
⬠	3.6
⊟	2.6
◇	1.6

M = 0.70

	Nominal $p_{t,p}/p_\infty$
O	1.2
□	1.6
◇	2.0
△	2.9
◁	3.3
⬠	2.6
⊟	1.9
◇	1.4

M = 0.50

	Nominal $p_{t,p}/p_\infty$
O	1.2
□	1.6
◇	2.0
△	2.9
◁	3.2
⬠	2.6
⊟	1.9
◇	1.4

M = 0.90

	Nominal $p_{t,p}/p_\infty$
O	1.6
□	2.0
◇	2.9
△	3.3
◁	2.6
⬠	1.8
⊟	1.4

Ejector pressure ratio, $p_{t,s}/p_{t,p}$

Corrected secondary weight-flow ratio, $\omega\sqrt{\frac{\tau}{\mu}}$

(b) Configuration M-13.

Figure 5.- Continued.

M = 0.70
Nominal
$p_{t,p}/p_\infty$
○ 1.2   △ 3.3
□ 1.6   ◁ 2.5
◇ 2.0   ◻ 1.9
△ 2.9   ◇ 1.4

M = 0.50
Nominal
$p_{t,p}/p_\infty$
○ 1.3   △ 3.3
□ 1.6   ◁ 2.5
◇ 2.0   ◻ 1.9
△ 2.9   ◇ 1.4

M = 0
Nominal
$p_{t,p}/p_\infty$
○ 1.4   △ 3.1
□ 1.7   ◁ 3.6
◇ 2.0   ◻ 2.6
△ 2.5

Corrected secondary weight-flow ratio, $\omega_4\sqrt{\frac{T}{\mu}}$

Ejector pressure ratio, $p_{t,s}/p_{t,p}$

(c) Configuration M-21.
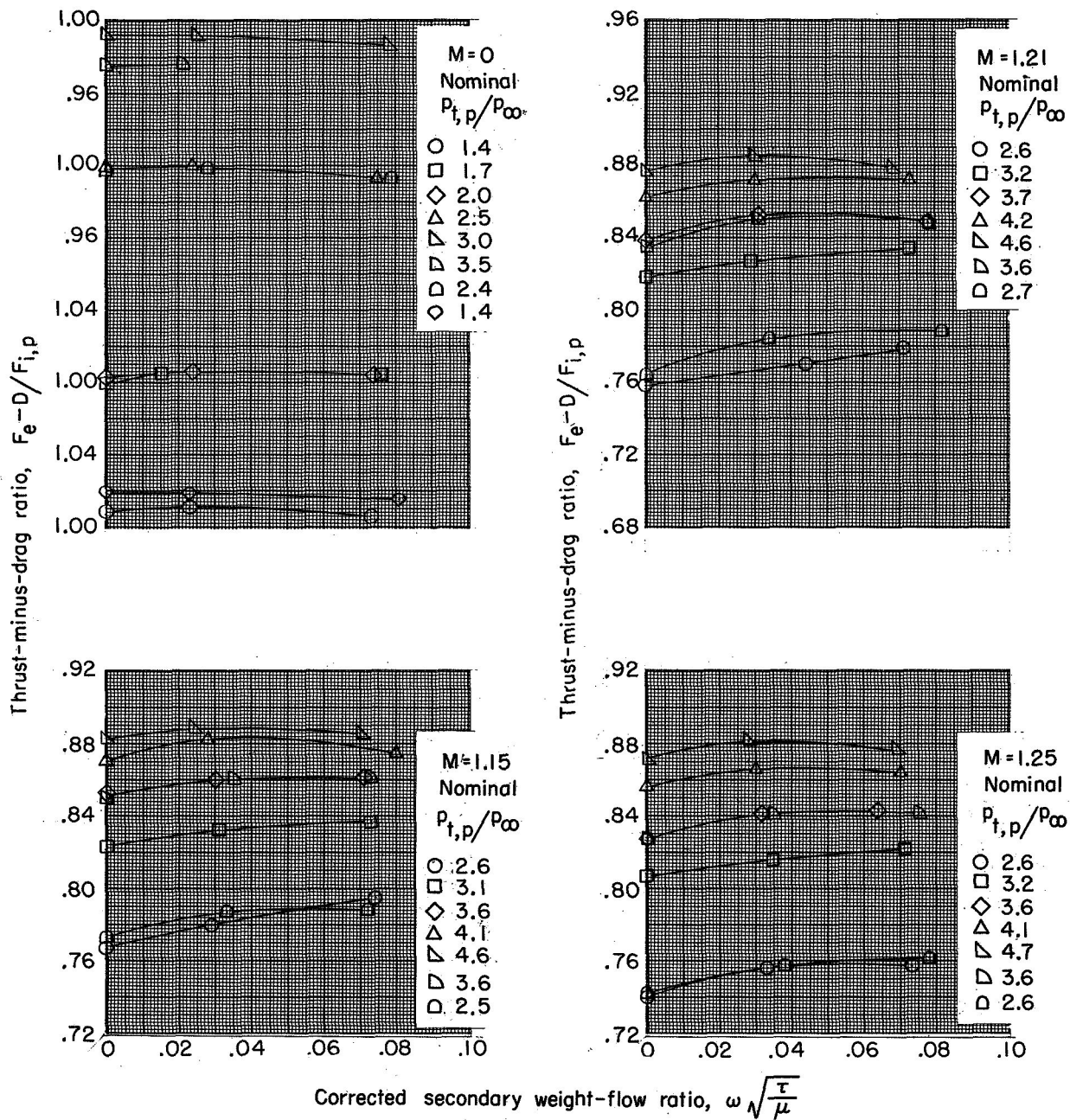
Figure 5.- Continued.

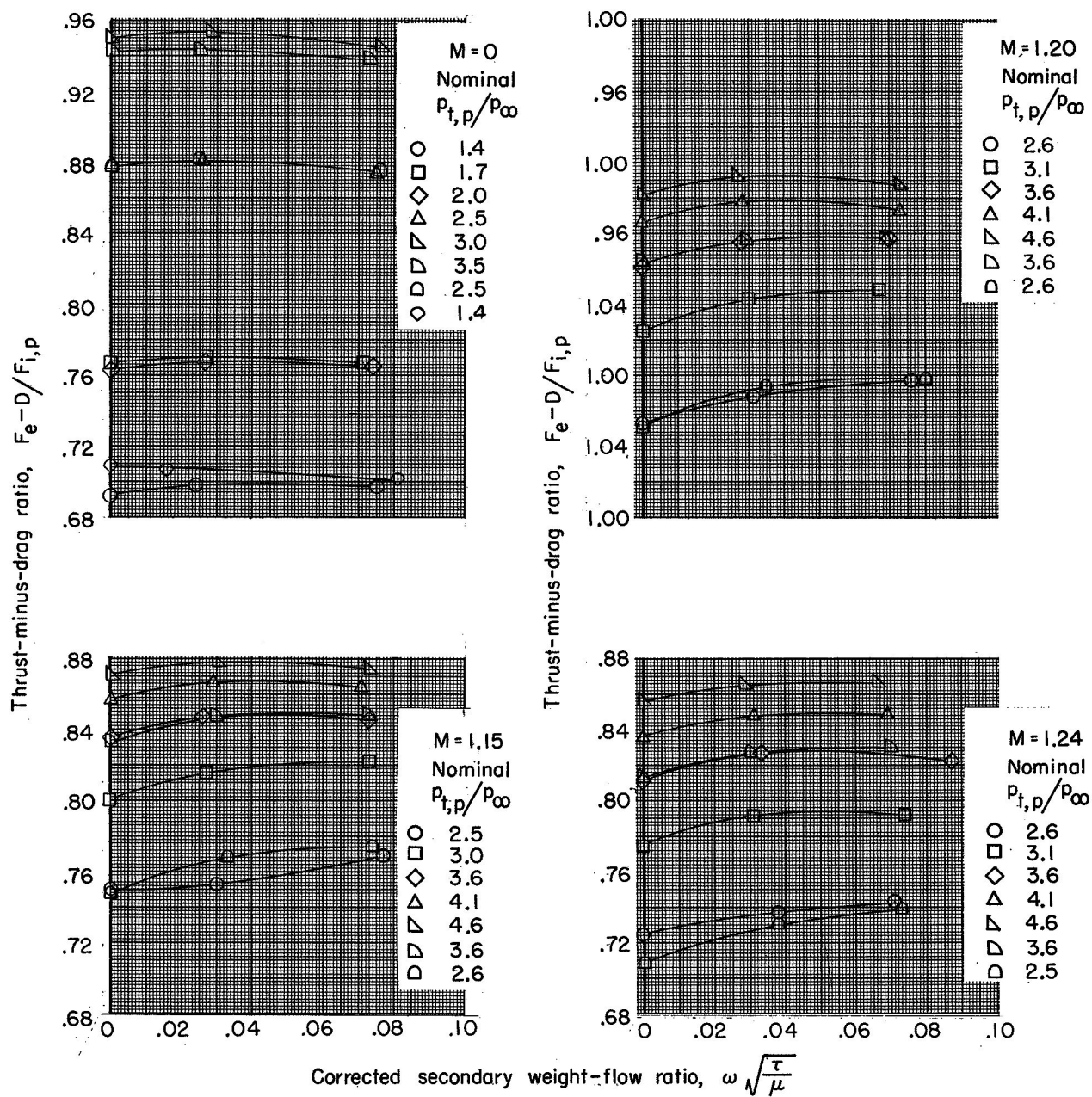19
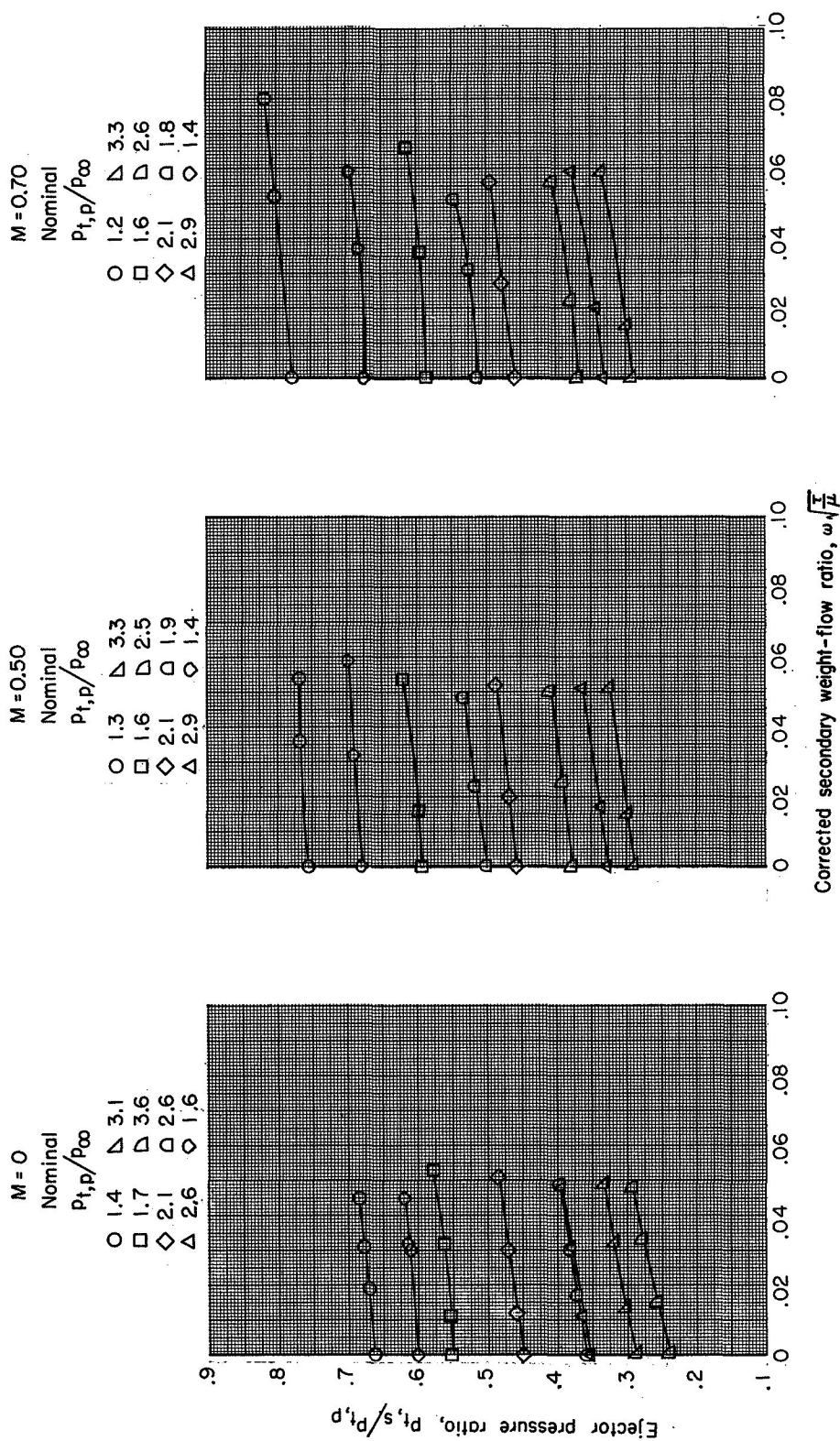
(d) Configuration M-3L.

Figure 5.- Continued.
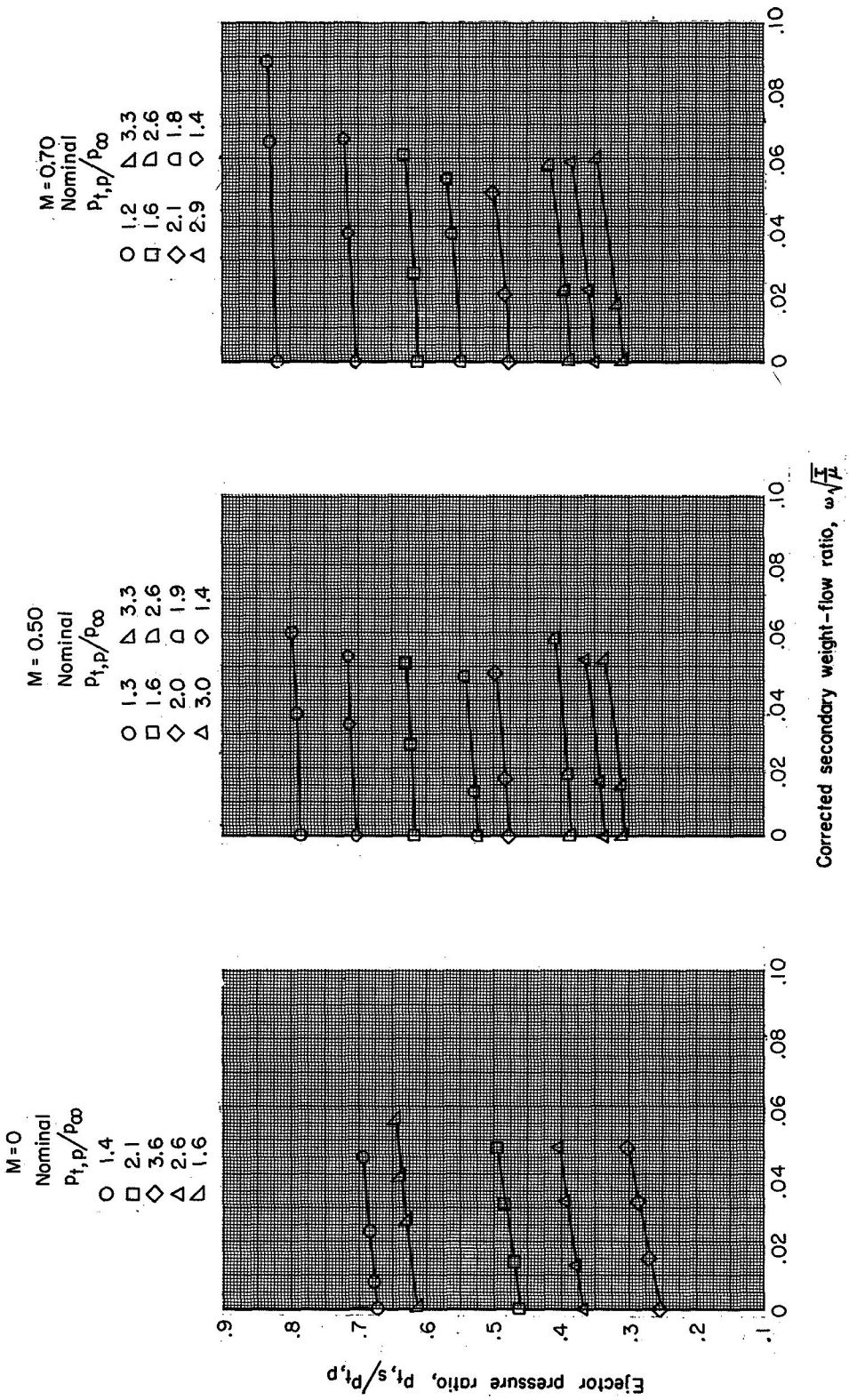
(e) Configuration M-23.
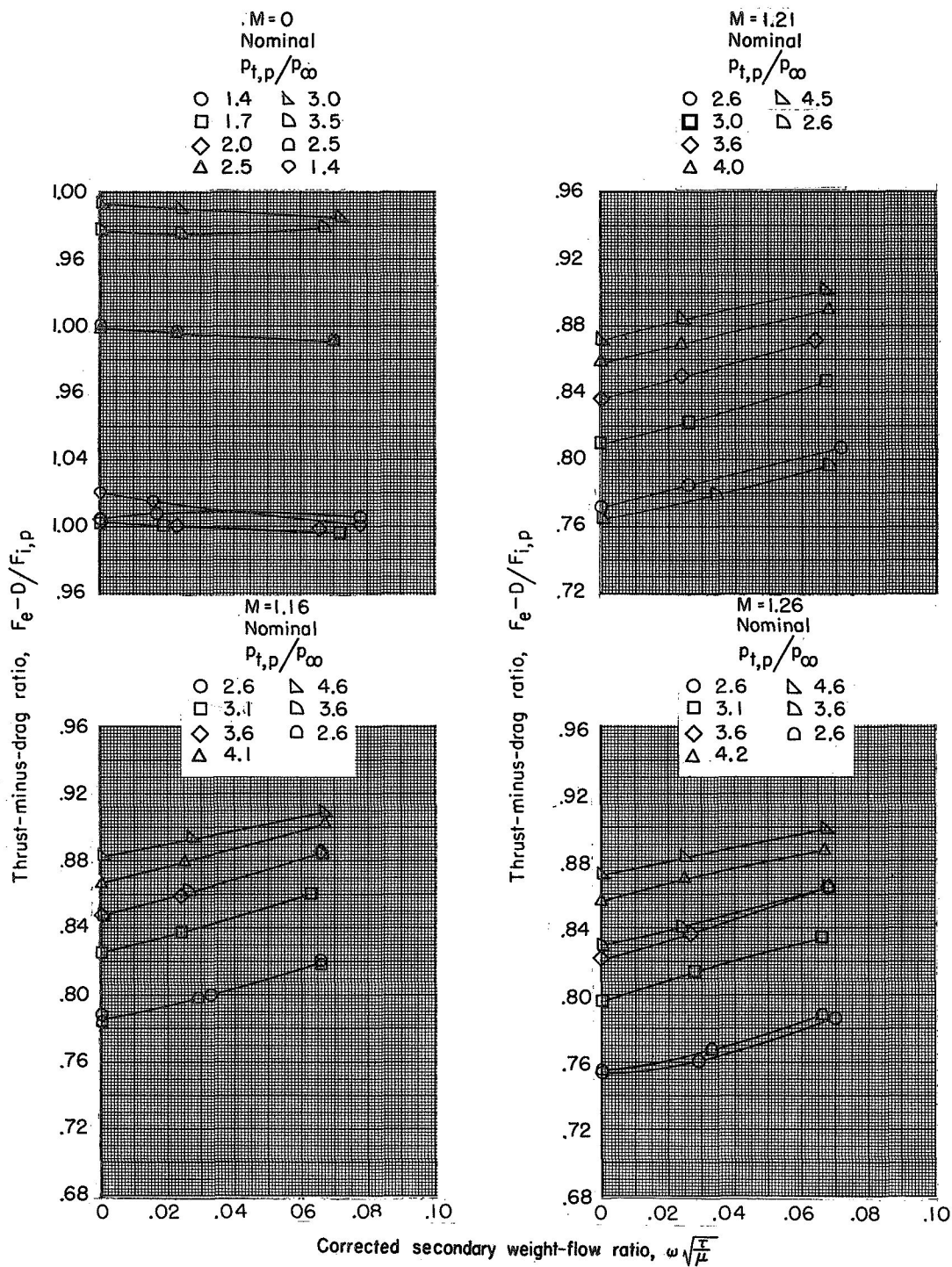
Figure 5.- Continued.
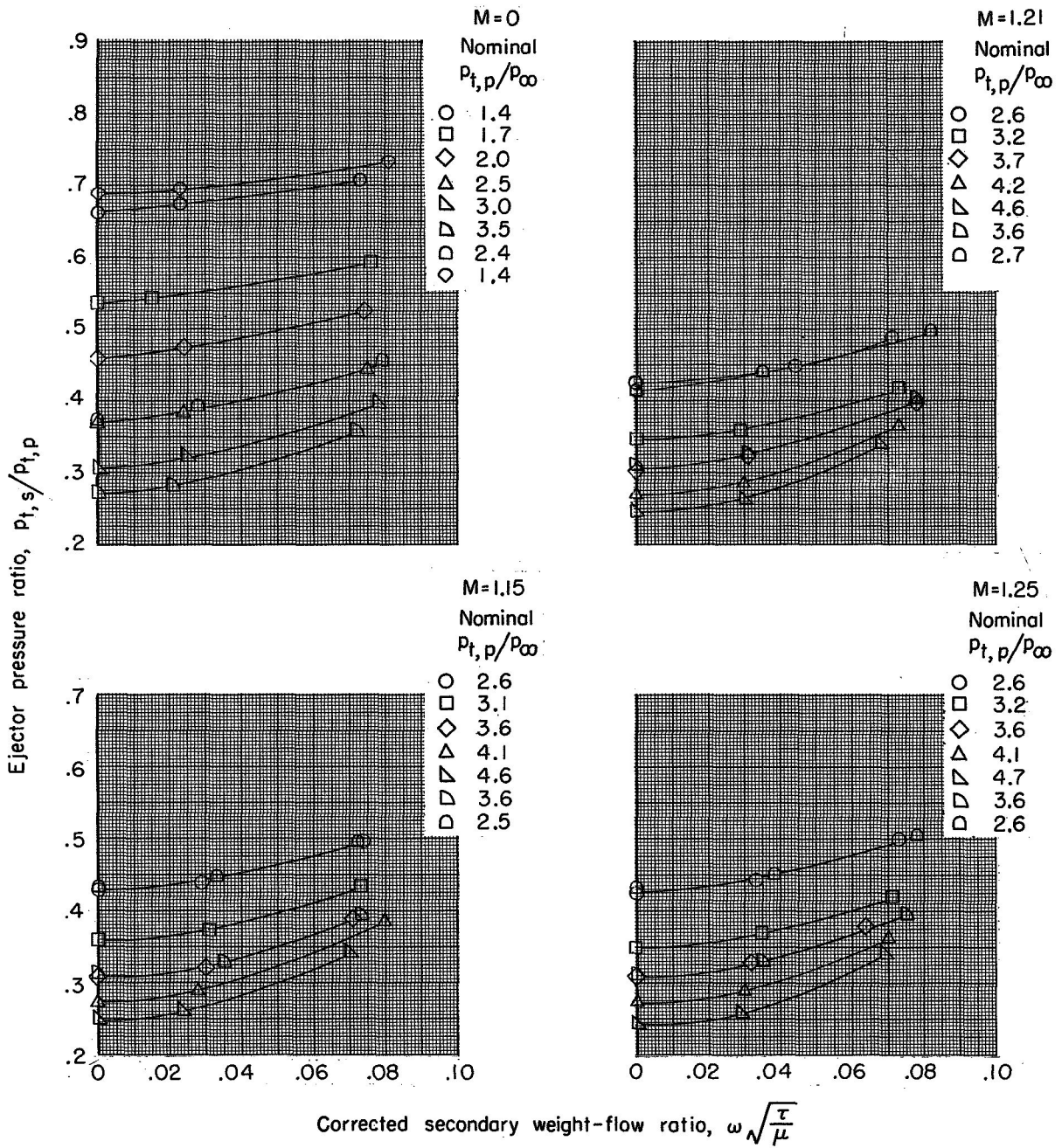
(f) Configuration A-11.
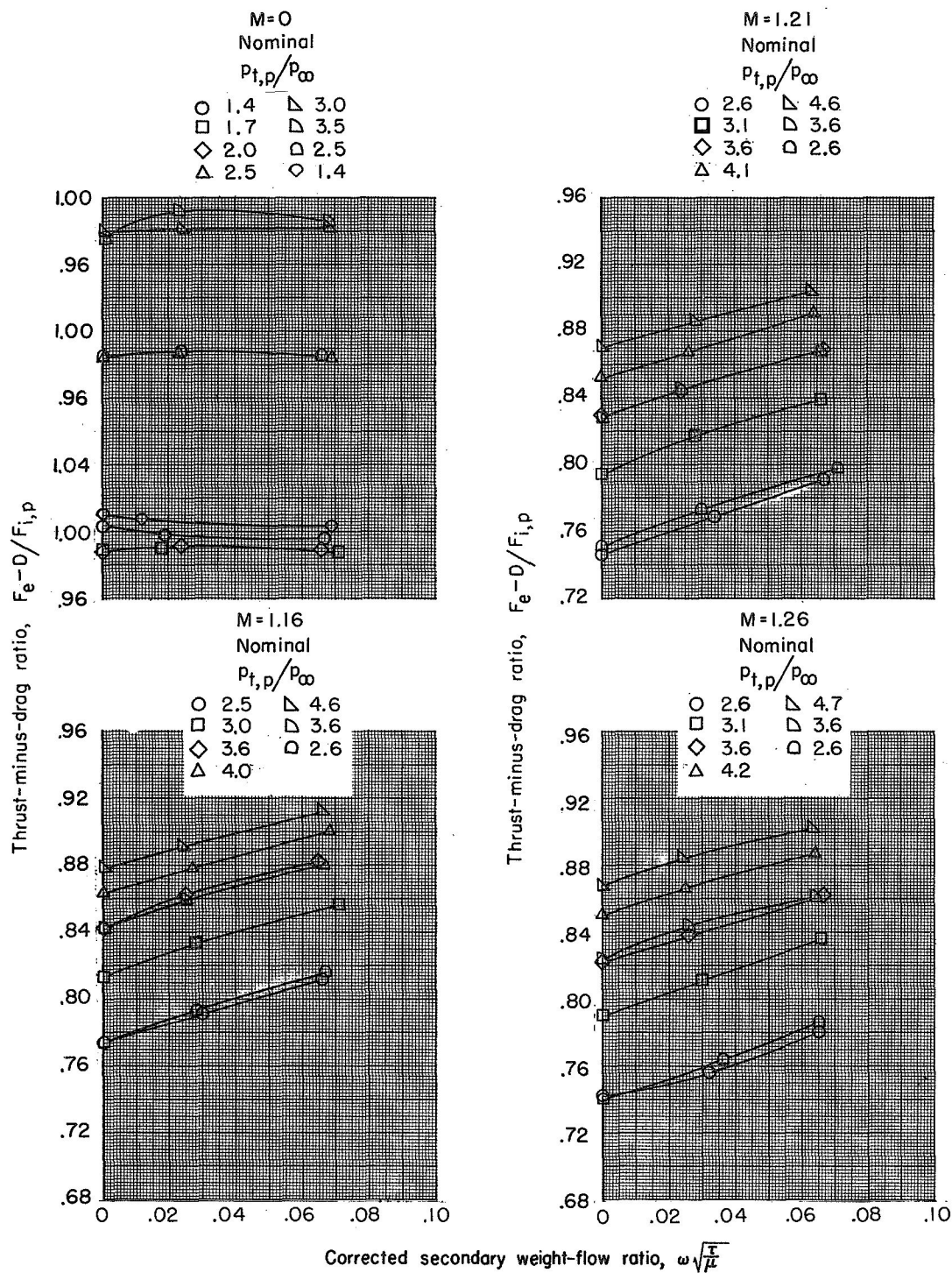
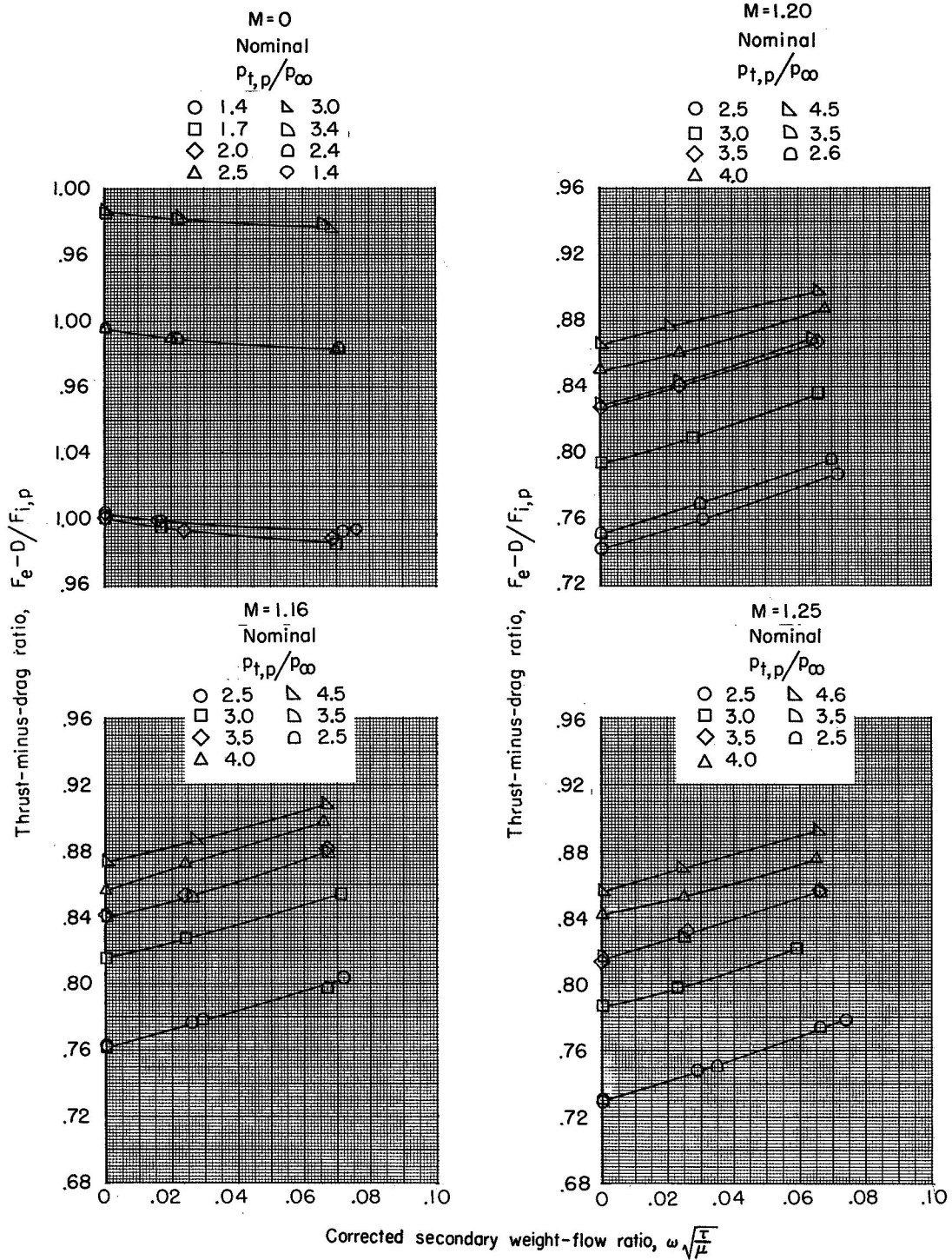Figure 5.- Continued.
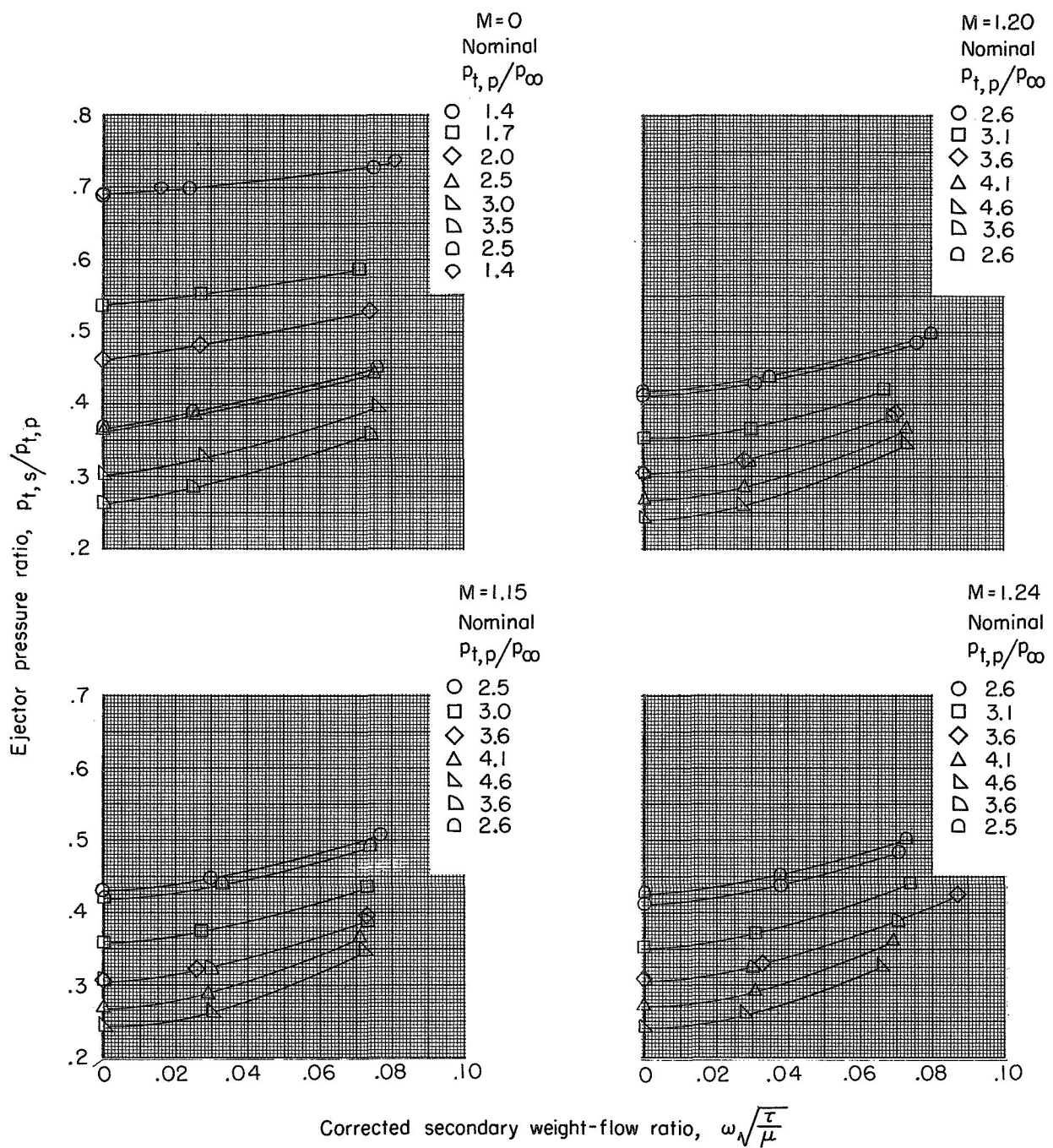
(g) Configuration A-13.

Figure 5.- Continued.
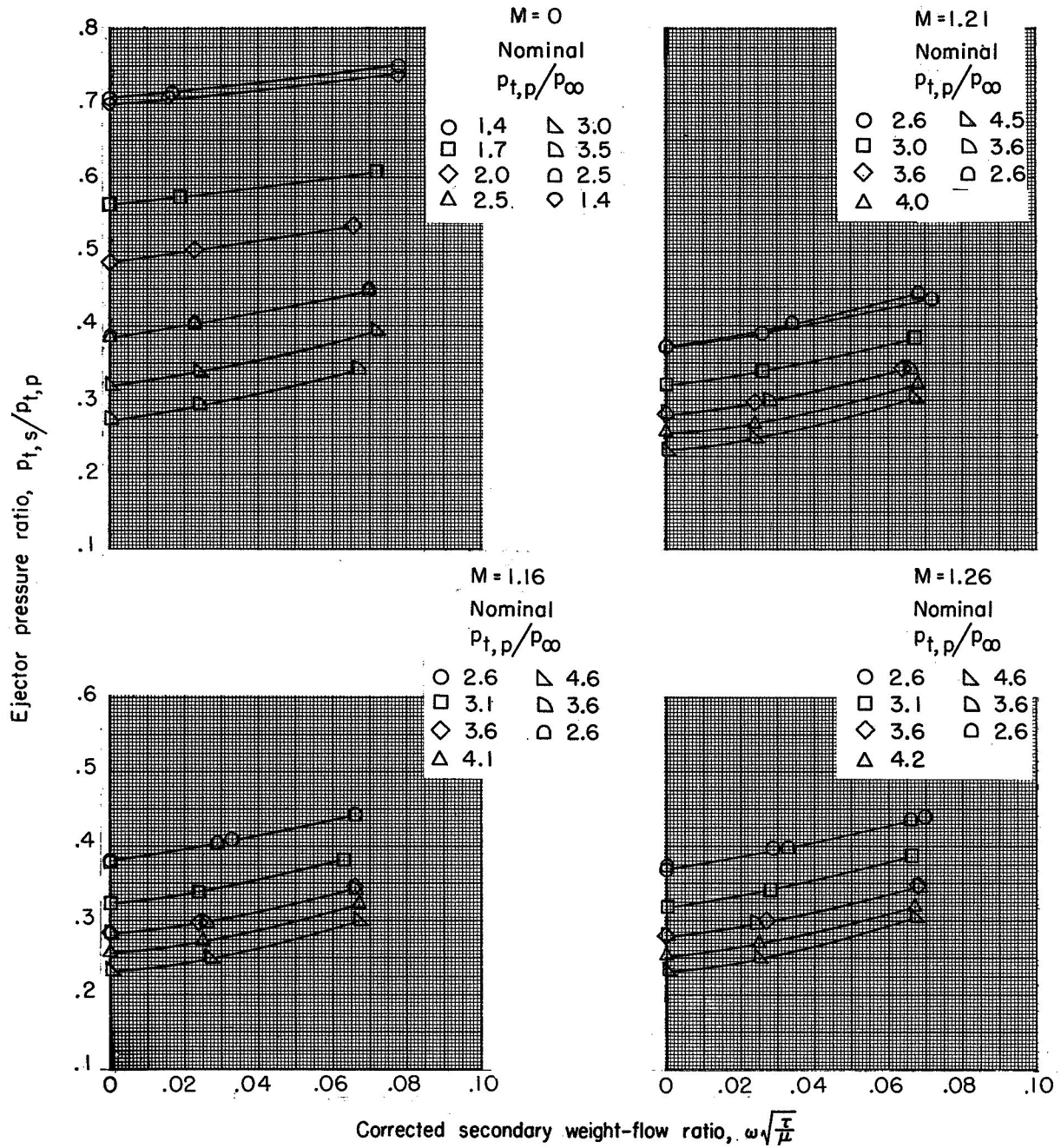
(h) Configuration A-21.

Figure 5.- Continued.
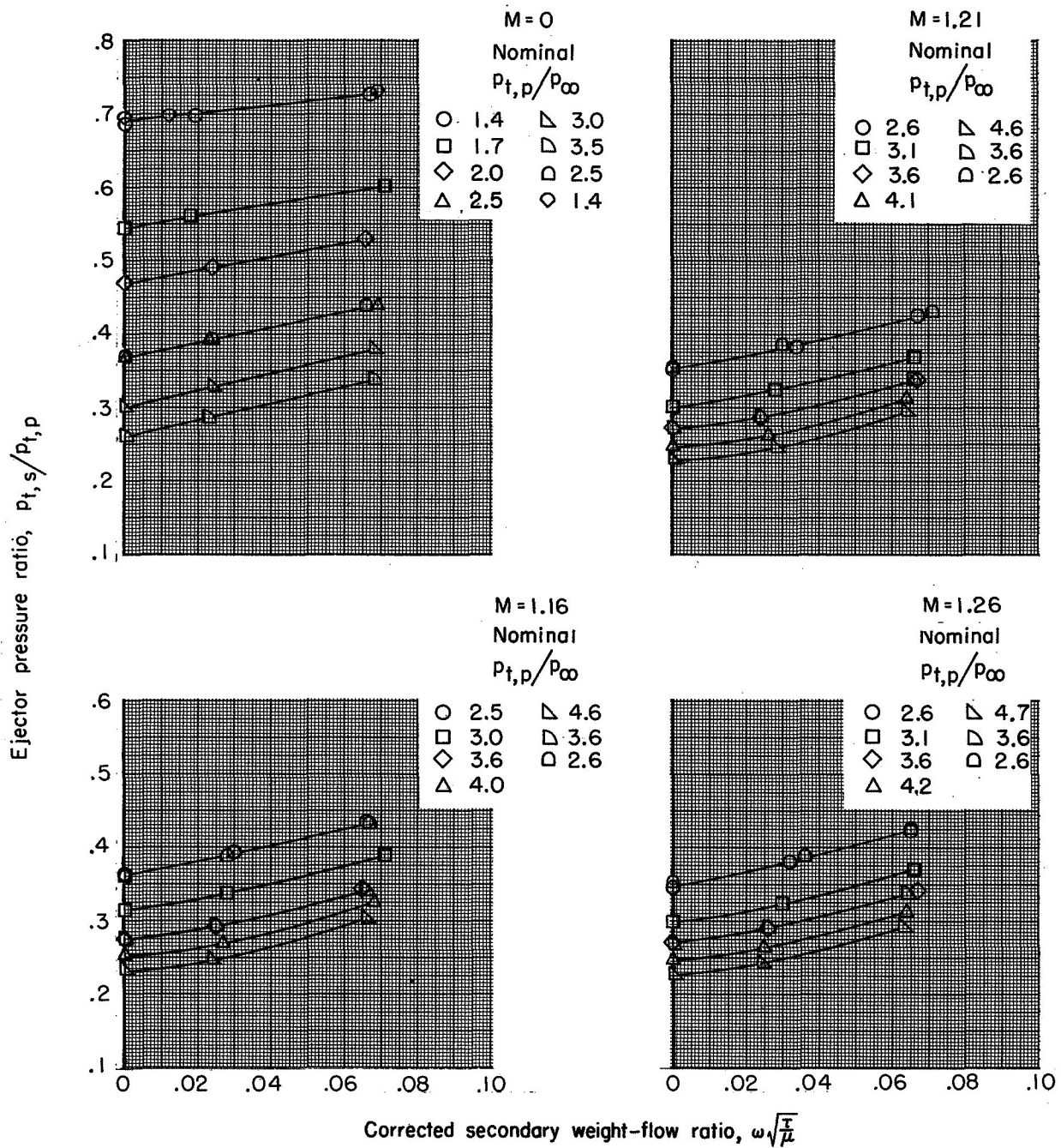
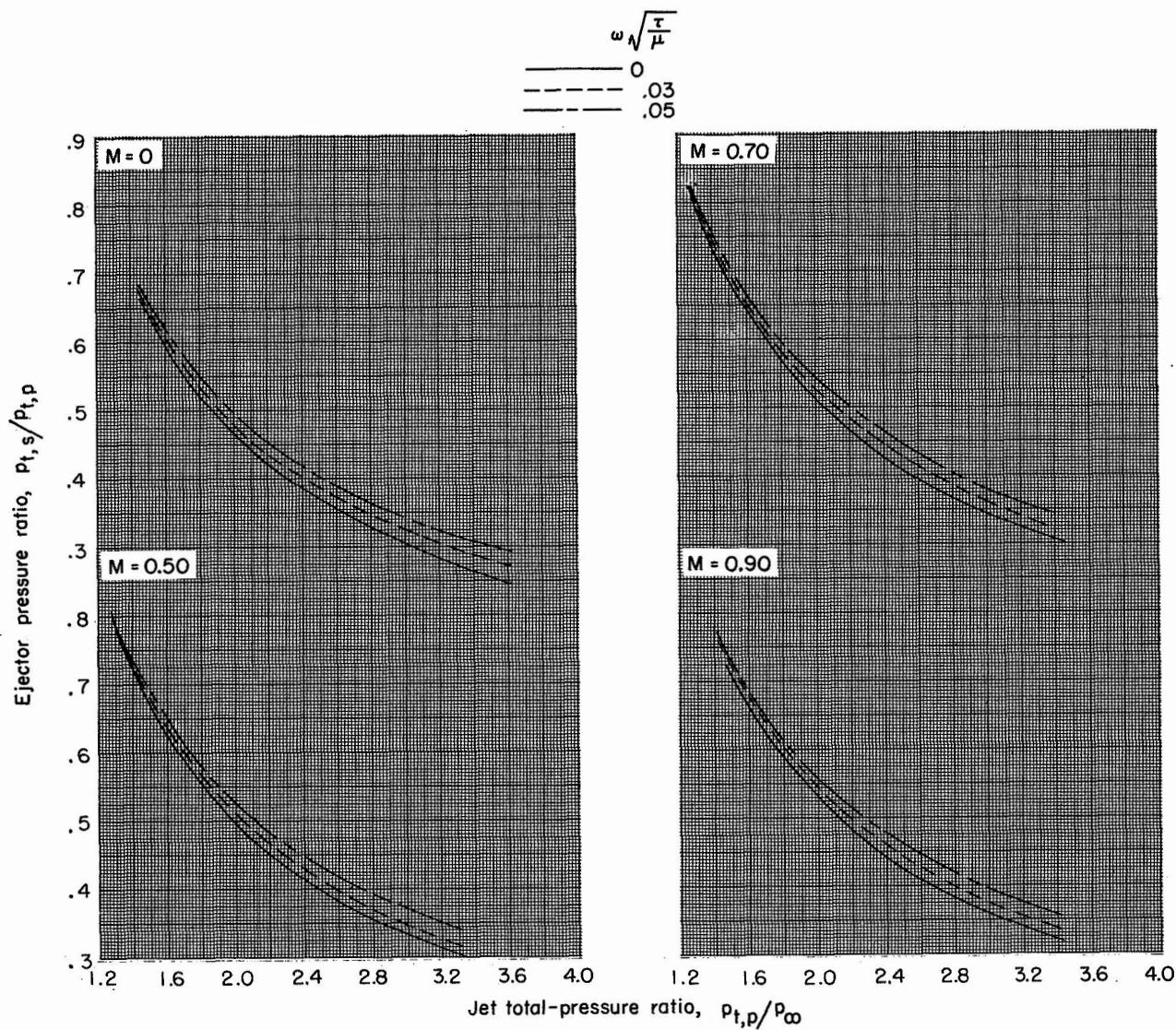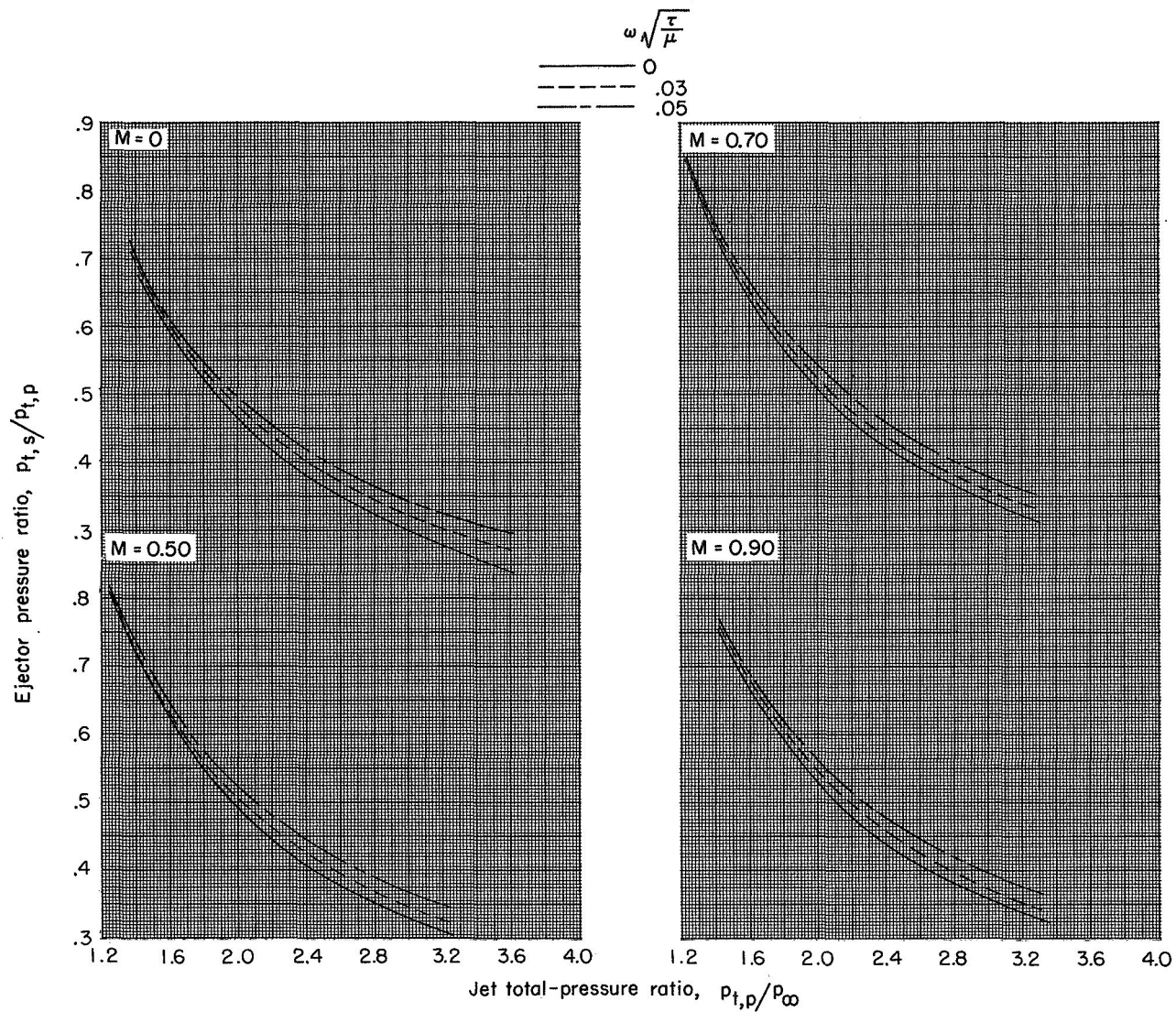(i) Configuration A-31.

Figure 5.- Continued.

M = 0
Nominal
$p_{t,p}/p_\infty$

O	1.4	△	3.0
□	1.7	◁	3.4
◇	2.0	◻	2.4
△	2.5	◇	1.4

M = 1.20
Nominal
$p_{t,p}/p_\infty$

O	2.5	△	4.5
□	3.0	◁	3.5
◇	3.5	◻	2.6
△	4.0		

M = 1.16
Nominal
$p_{t,p}/p_\infty$

O	2.5	△	4.5
□	3.0	◁	3.5
◇	3.5	◻	2.5
△	4.0		

M = 1.25
Nominal
$p_{t,p}/p_\infty$

O	2.5	△	4.6
□	3.0	◁	3.5
◇	3.5	◻	2.5
△	4.0		

Ejector pressure ratio, $p_{t,s}/p_{t,p}$

Corrected secondary weight-flow ratio, $\omega\sqrt{\frac{\tau}{\mu}}$
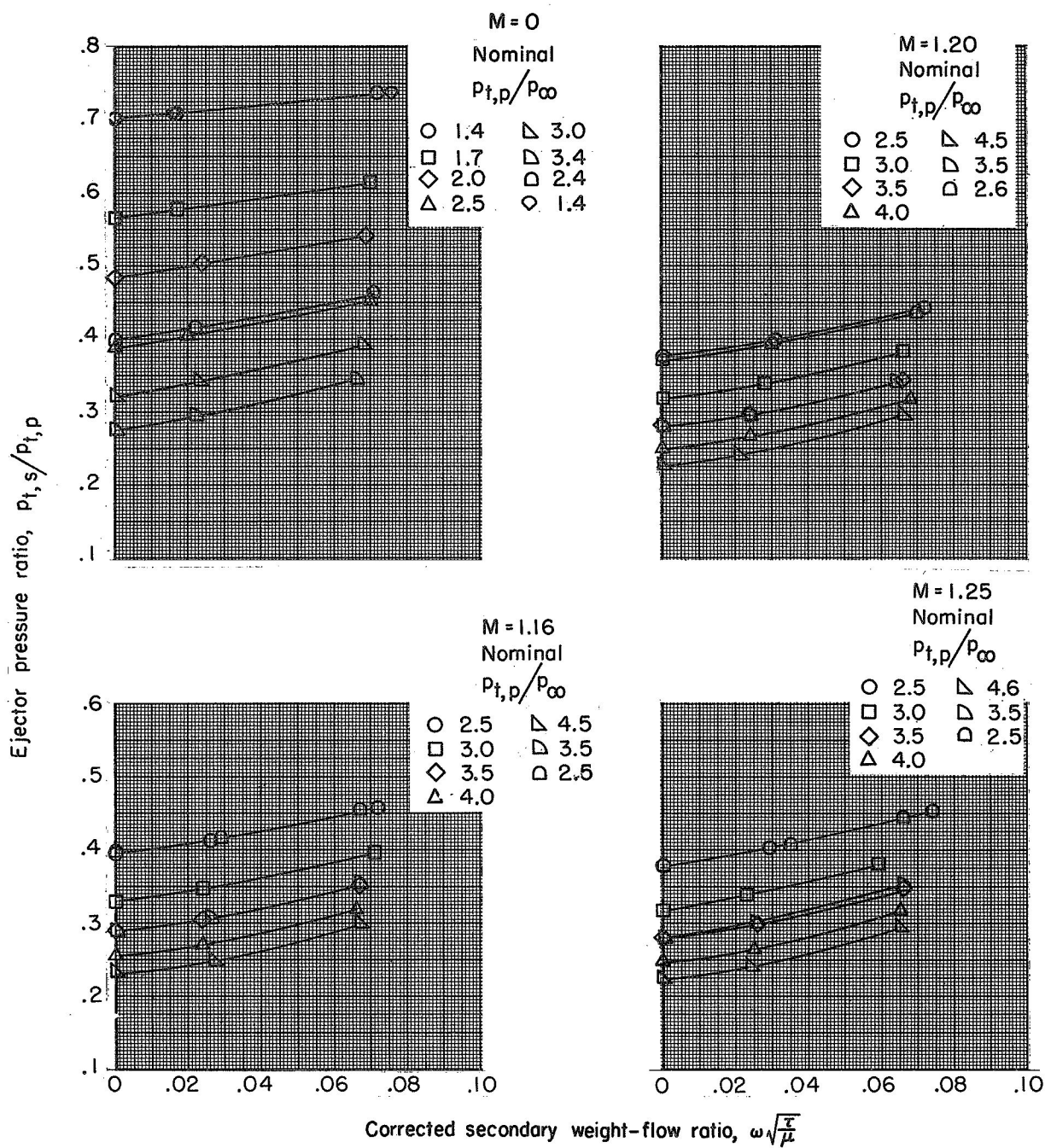
(j) Configuration A-23.

Figure 5.- Concluded.
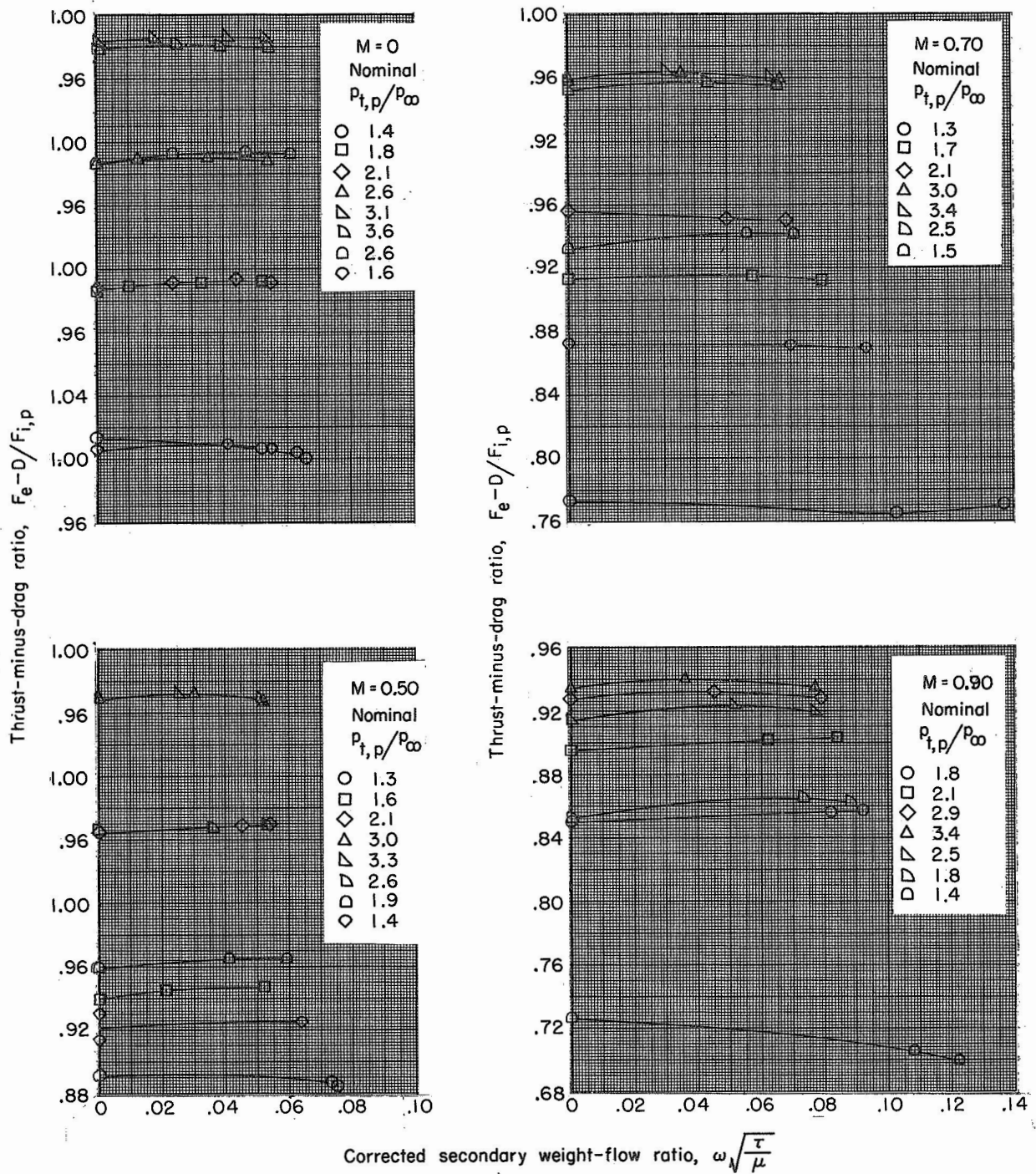
(a) Configuration M-11.

Figure 6.- Gross ejector thrust-minus-drag ratio as a function of corrected weight-flow ratio for various primary total-pressure ratios and Mach numbers.
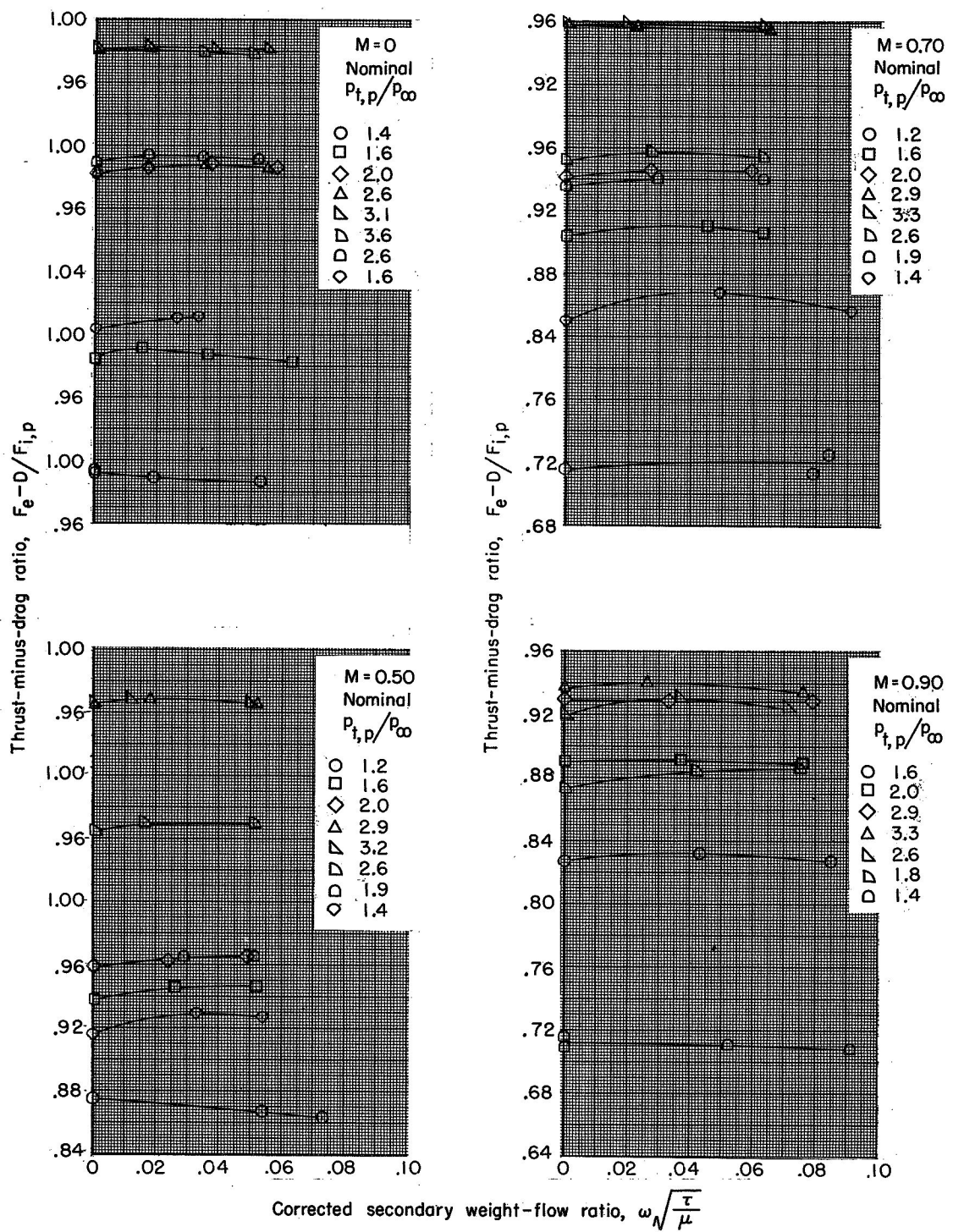
(b) Configuration M-13.

Figure 6.- Continued.

M = 0.70
Nominal
$p_{t,p}/p_\infty$

O 1.2   △ 3.3
□ 1.6   ◁ 2.5
◇ 2.0   ◇ 1.9
△ 2.9   ○ 1.4

Thrust-minus-drag ratio, $F_e - D/F_{i,p}$

1.00 .96 .92 .96 .92 .88 .84 .80 .76

0 .02 .04 .06 .08 .10

M = 0.50
Nominal
$p_{t,p}/p_\infty$

O 1.3   △ 3.3
□ 1.6   ◁ 2.5
◇ 2.0   ◇ 1.9
△ 2.9   ○ 1.4

Thrust-minus-drag ratio, $F_e - D/F_{i,p}$

1.00 .96 1.00 .96 1.00 .96 .92 .88 .84

Corrected secondary weight-flow ratio, $\omega\sqrt{\frac{\tau}{\mu}}$

0 .02 .04 .06 .08 .10

M = 0
Nominal
$p_{t,p}/p_\infty$

O 1.4   △ 3.1
□ 1.7   ◁ 3.6
◇ 2.0   ◻ 2.6
△ 2.5

Thrust-minus-drag ratio, $F_e - D/F_{i,p}$

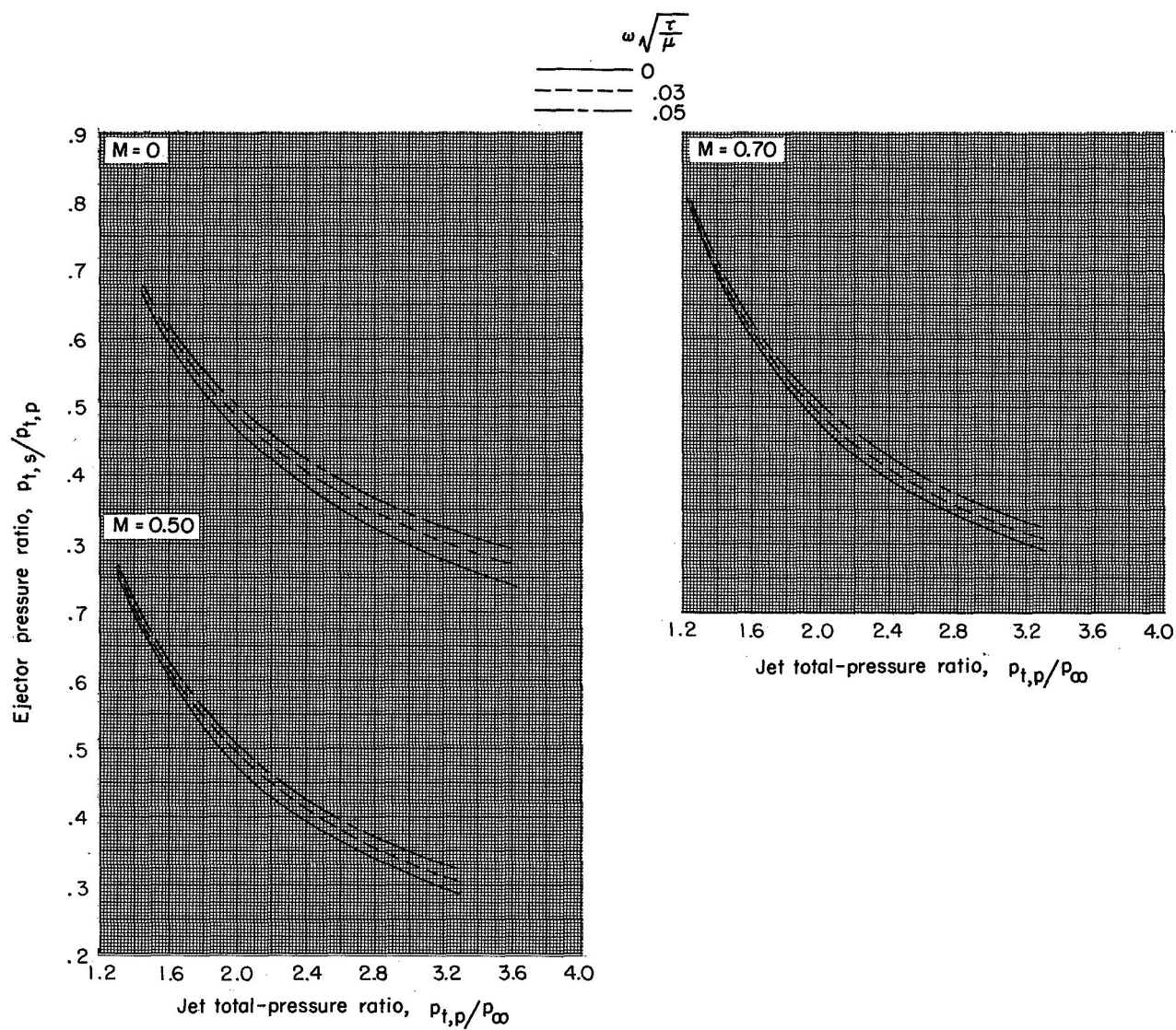1.00 .96 1.04 1.00 .96 1.04 1.00 .96 .92

0 .02 .04 .06 .08 .10
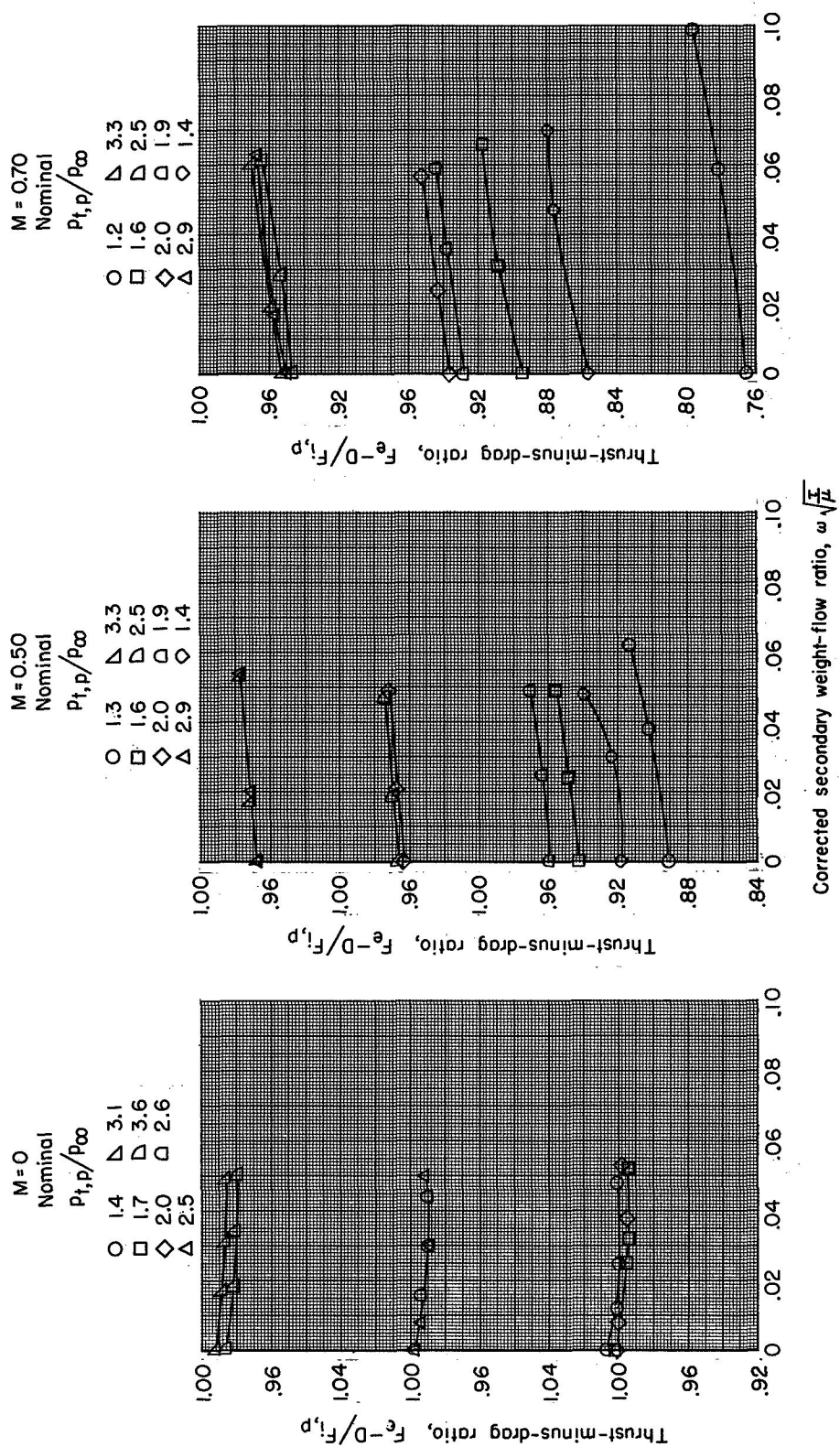
(c) Configuration M-21.

Figure 6.- Continued.
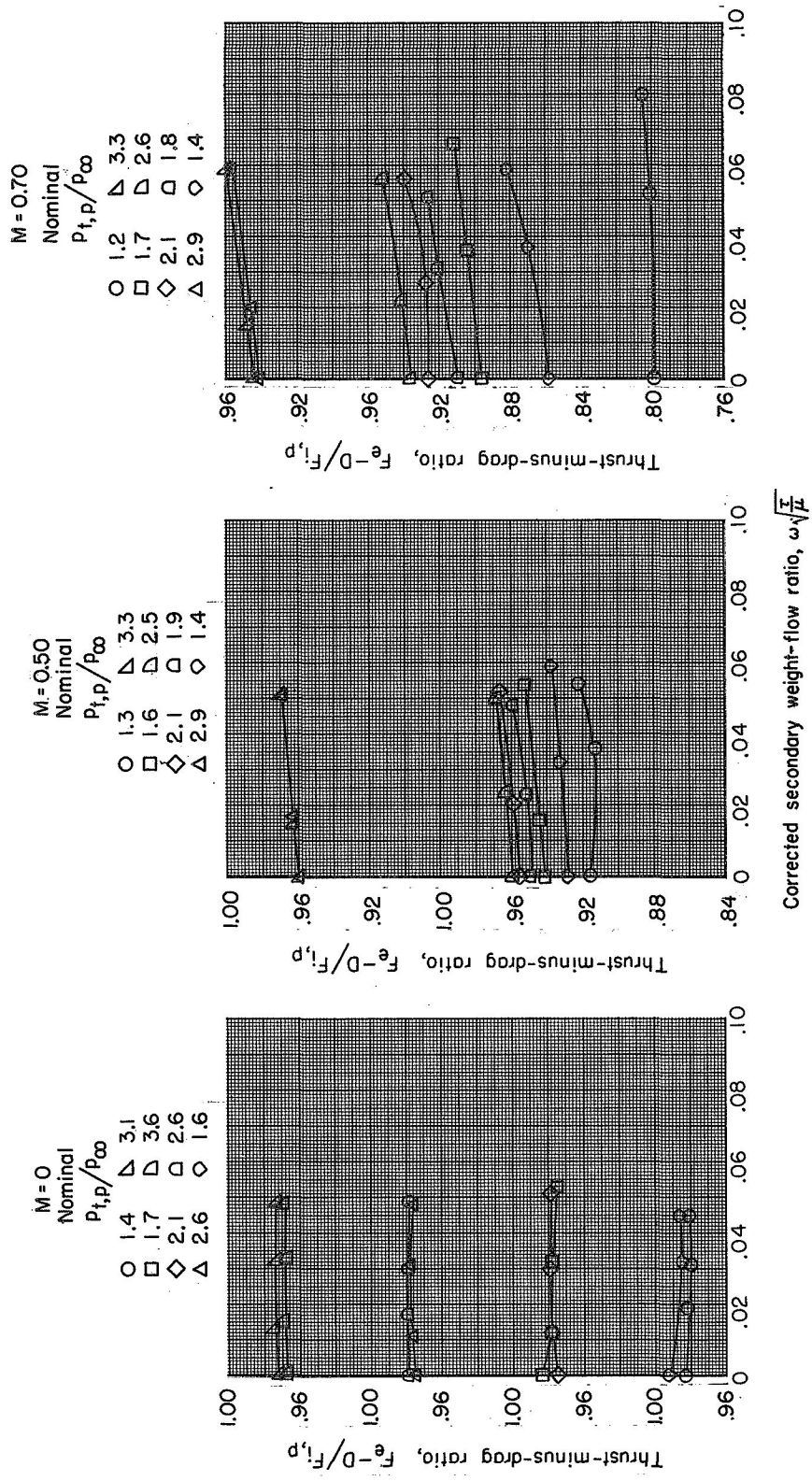
(d) Configuration M-31.

Figure 6.- Continued.
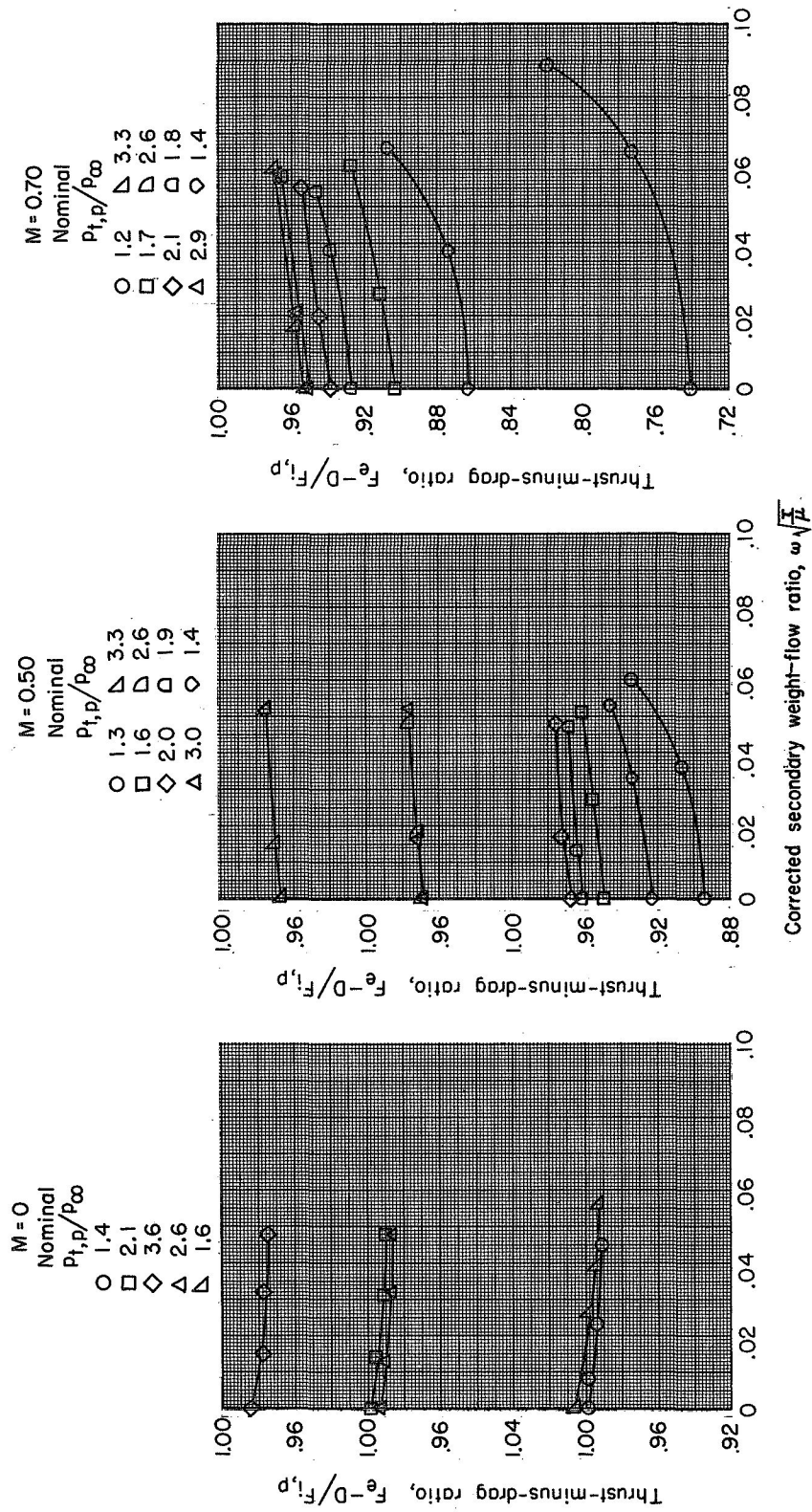
(e) Configuration M-23.

Figure 6.- Continued.

(f) Configuration A-11.

Figure 6.- Continued.

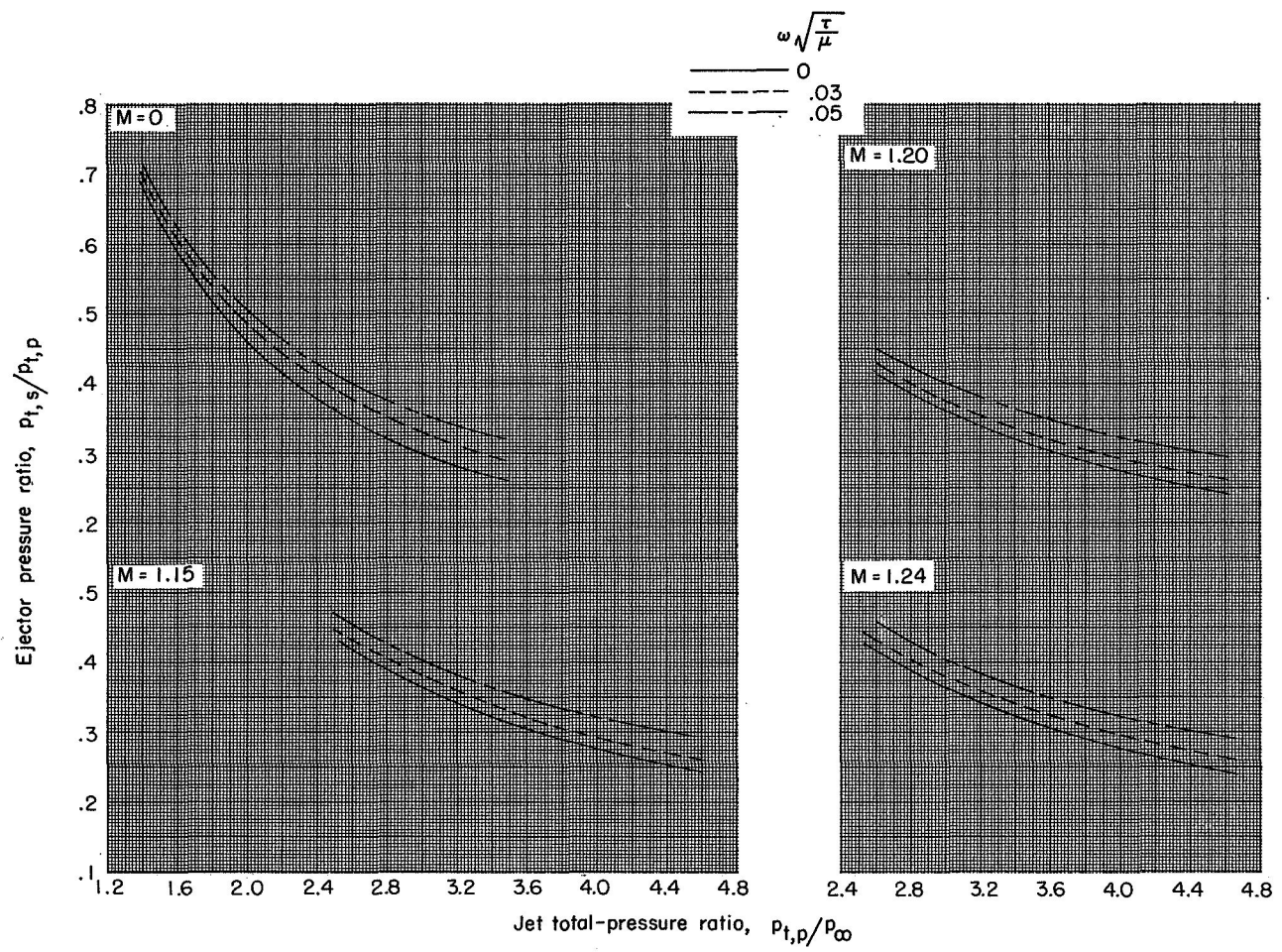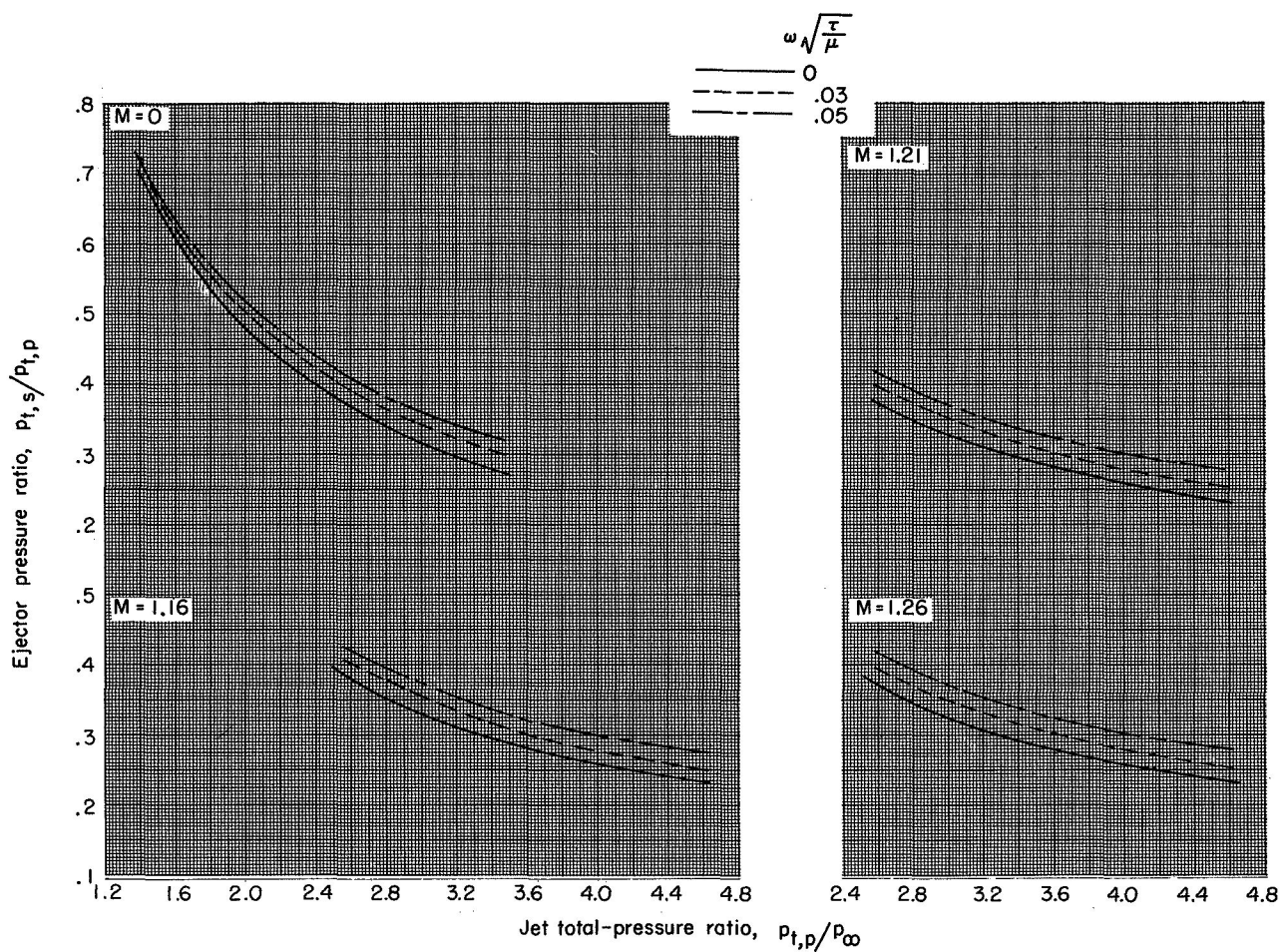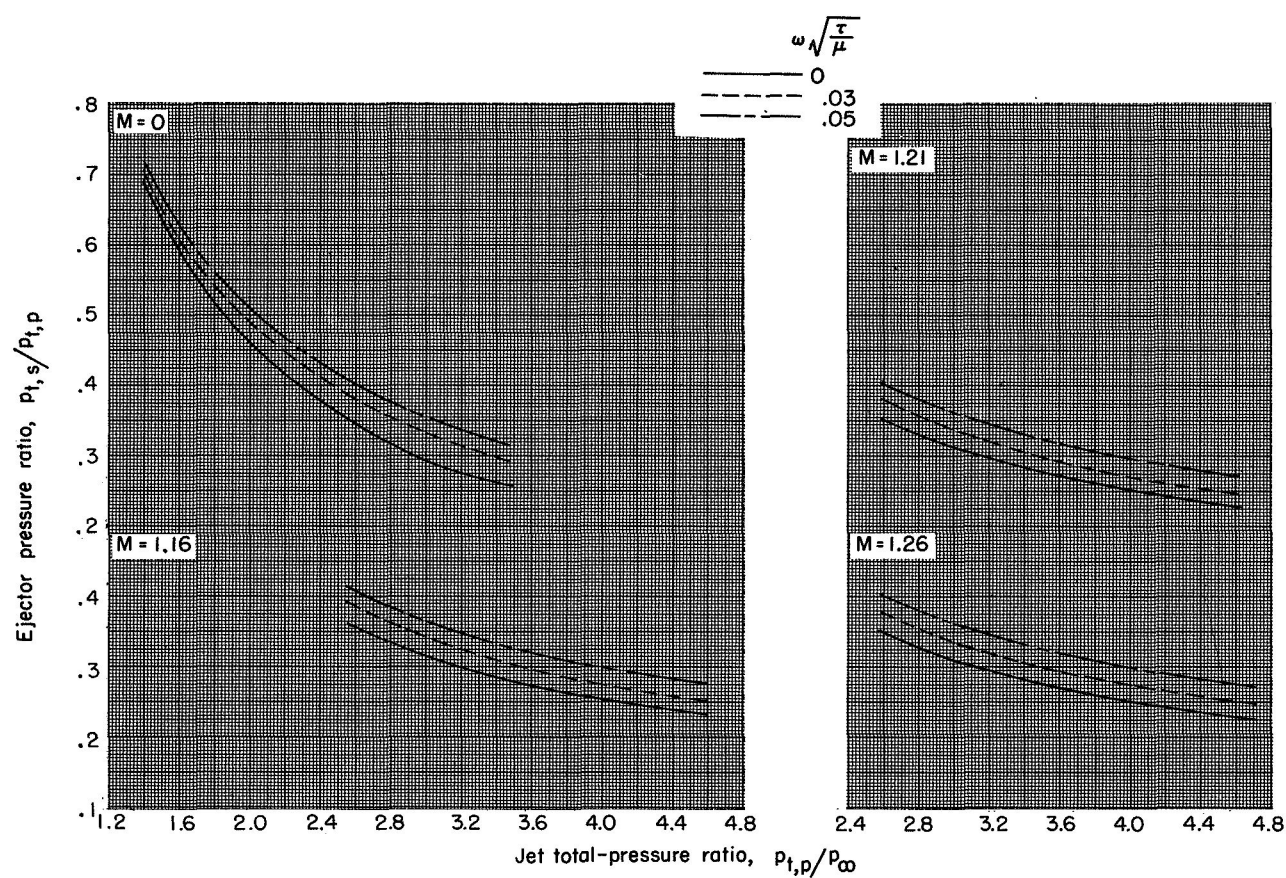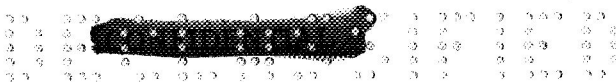(g) Configuration A-13.

Figure 6.- Continued.

M = 0
Nominal
$p_{t,p}/p_\infty$

O	1.4	◣	3.0
□	1.7	◪	3.5
◇	2.0	◓	2.5
△	2.5	◇	1.4

M = 1.21
Nominal
$p_{t,p}/p_\infty$

O	2.6	◣	4.5
◪	3.0	◪	2.6
◇	3.6		
△	4.0		

M = 1.16
Nominal
$p_{t,p}/p_\infty$

O	2.6	◣	4.6
□	3.1	◪	3.6
◇	3.6	◓	2.6
△	4.1		

M = 1.26
Nominal
$p_{t,p}/p_\infty$

O	2.6	◣	4.6
□	3.1	◪	3.6
◇	3.6	◓	2.6
△	4.2		

Thrust-minus-drag ratio, $F_e - D/F_{i,p}$

Corrected secondary weight-flow ratio, $\omega\sqrt{\frac{\tau}{\mu}}$

(h) Configuration A-21.

Figure 6.- Continued.

M = 0
Nominal
$p_{t,p}/p_\infty$

O	1.4	△	3.0
□	1.7	◁	3.5
◇	2.0	◹	2.5
△	2.5	◇	1.4

M = 1.21
Nominal
$p_{t,p}/p_\infty$

O	2.6	△	4.6
■	3.1	◁	3.6
◇	3.6	◹	2.6
△	4.1		

M = 1.16
Nominal
$p_{t,p}/p_\infty$

O	2.5	△	4.6
□	3.0	◁	3.6
◇	3.6	◹	2.6
△	4.0		

M = 1.26
Nominal
$p_{t,p}/p_\infty$

O	2.6	△	4.7
□	3.1	◁	3.6
◇	3.6	◹	2.6
△	4.2		

Thrust-minus-drag ratio, $F_e - D/F_{i,p}$

Corrected secondary weight-flow ratio, $\omega\sqrt{\frac{\tau}{\mu}}$

(i) Configuration A-31.

Figure 6.- Continued.

(j) Configuration A-23.
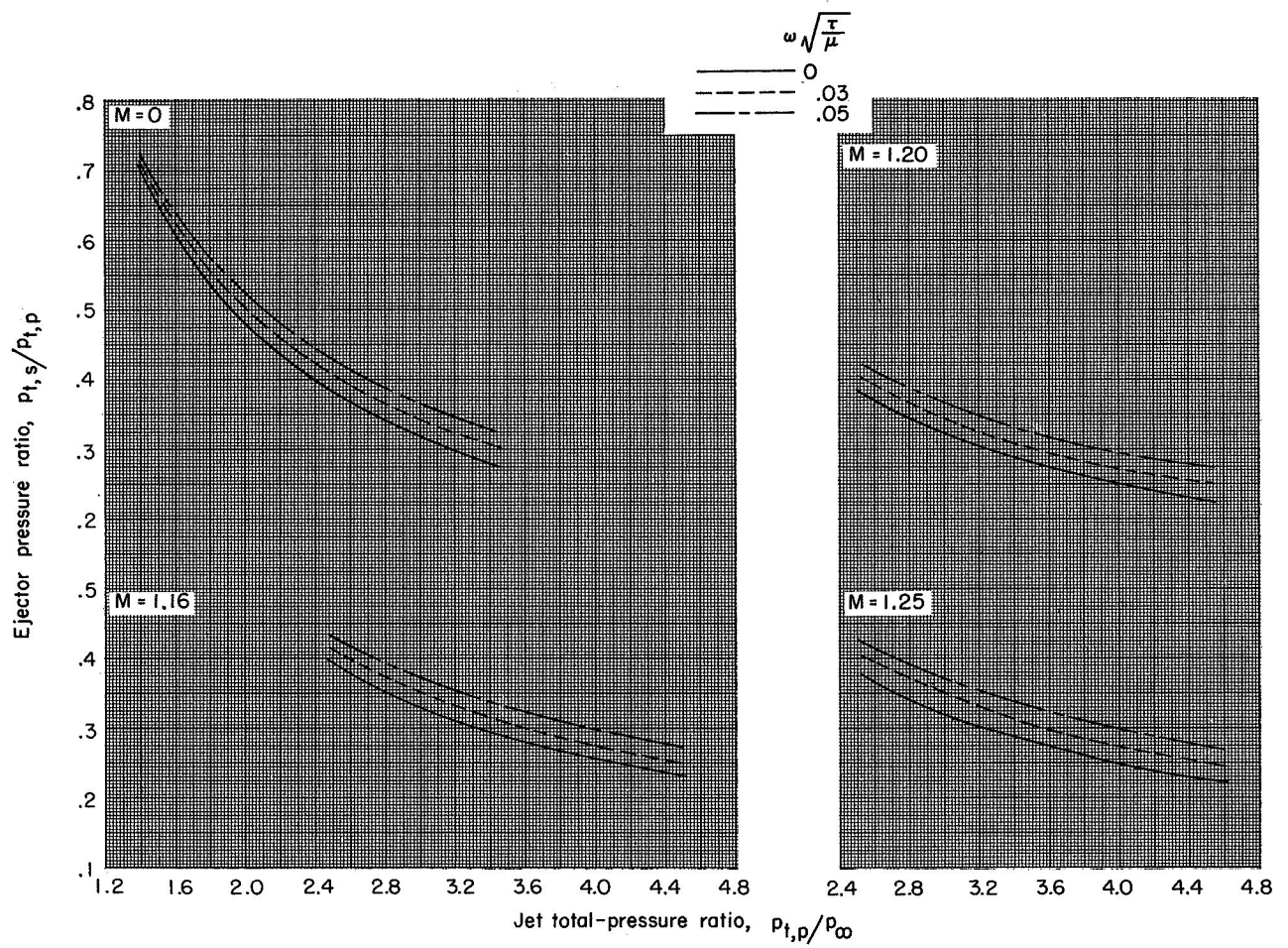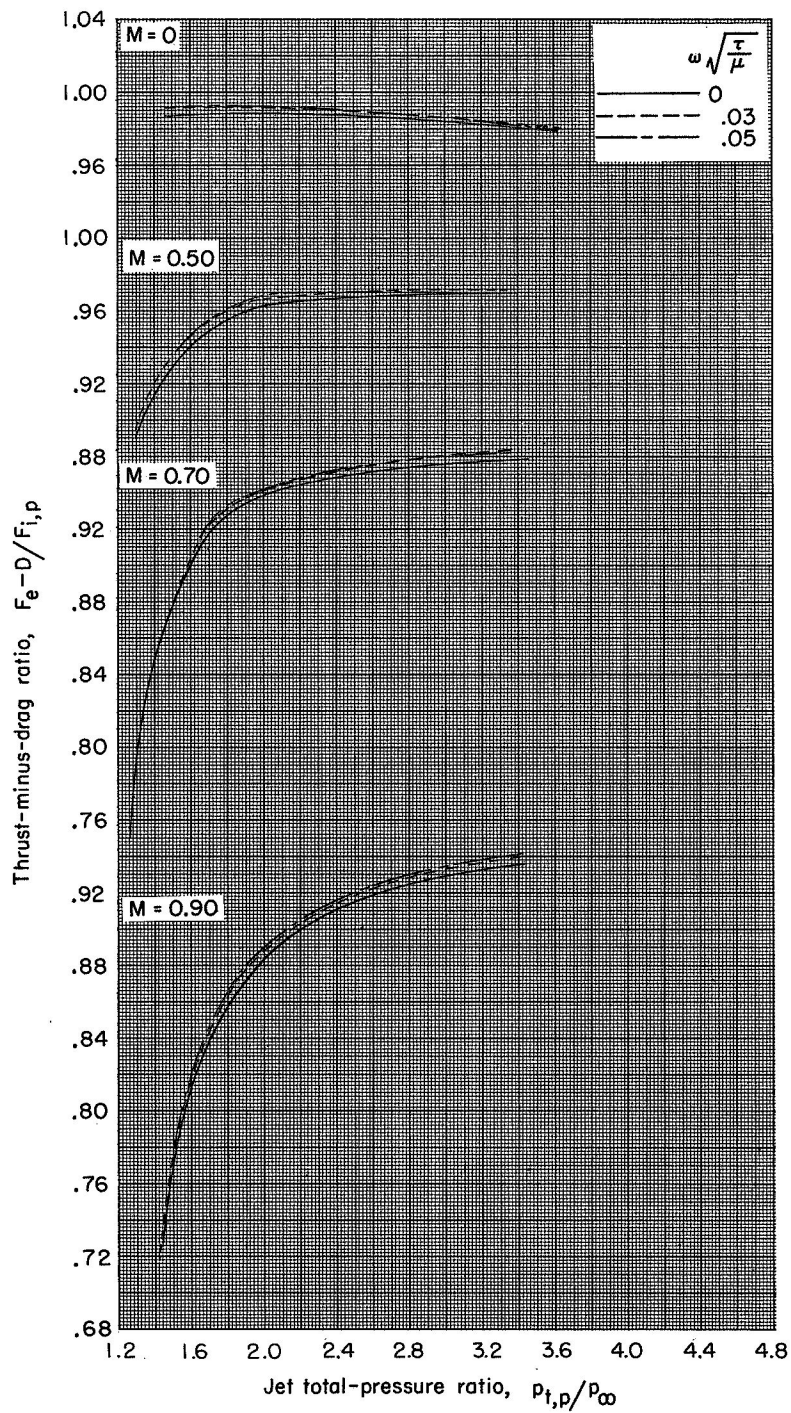
Figure 6.- Concluded.
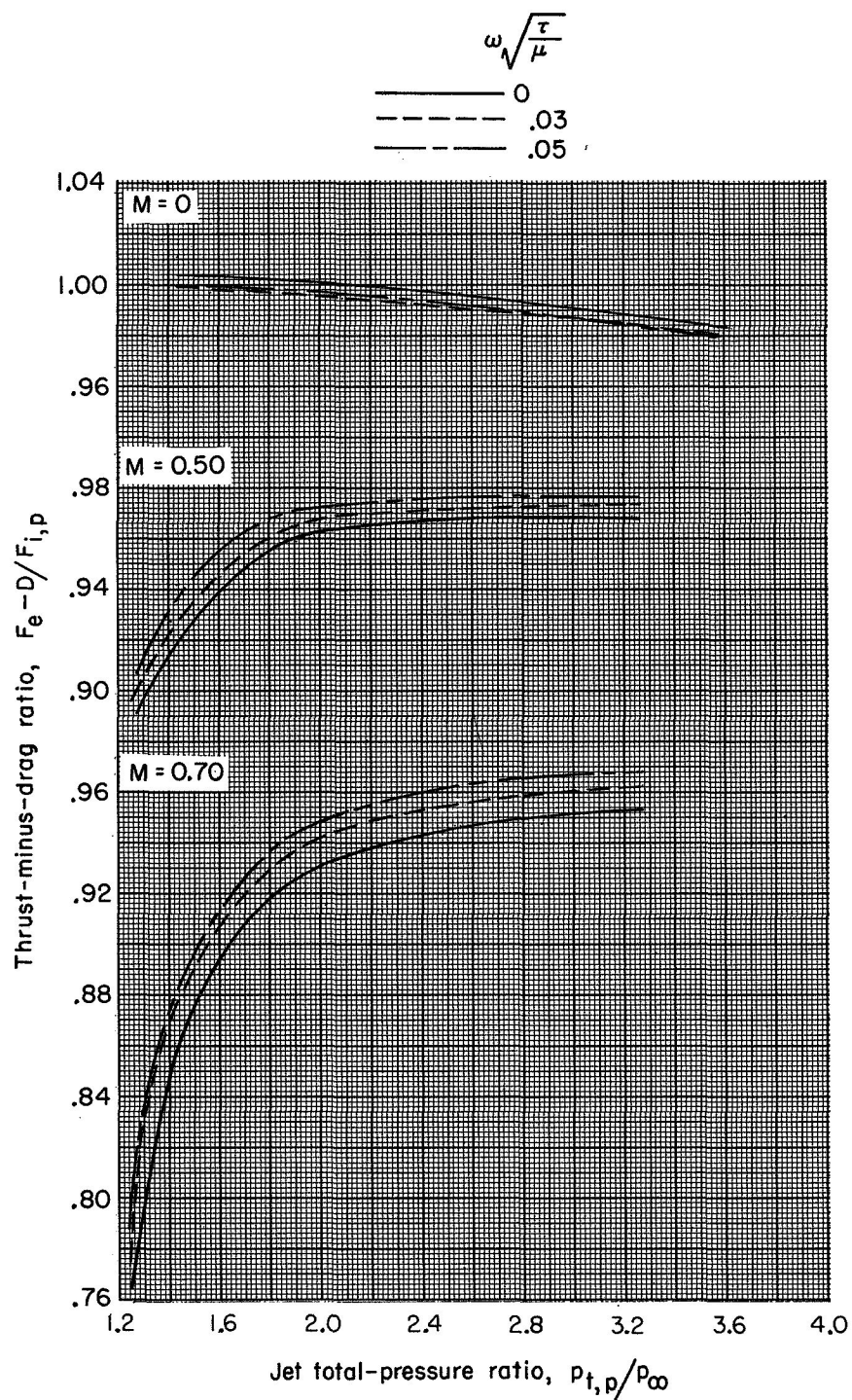
(a) Configuration M-11.

Figure 7.- Variation of ejector pressure ratio with primary total-pressure ratio for constant corrected weight-flow ratios and Mach numbers.

(b) Configuration M-13.

Figure 7.- Continued.
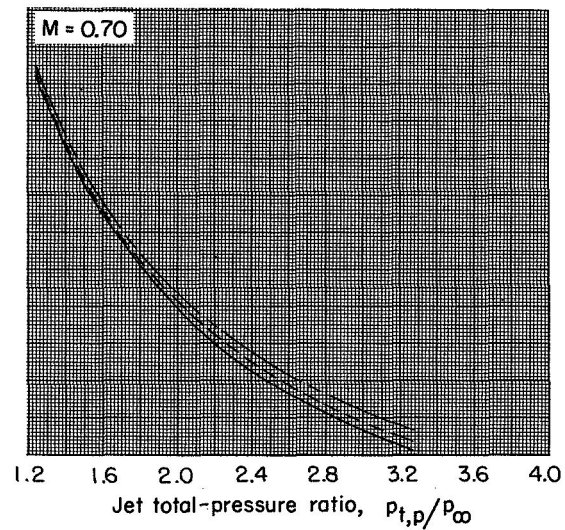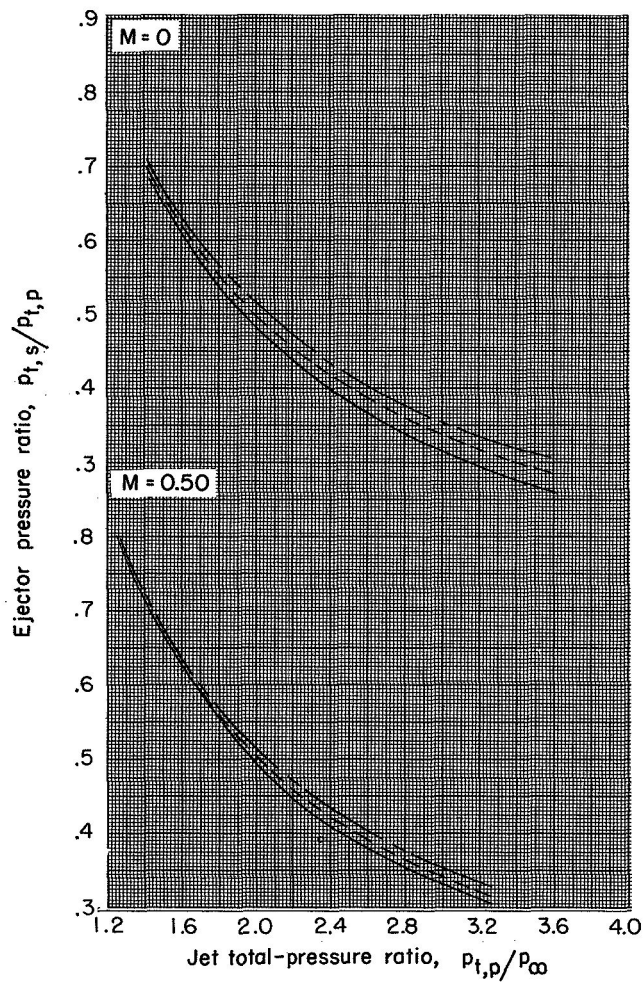
(c) Configuration M-21.

Figure 7.- Continued.

$\omega\sqrt{\dfrac{\tau}{\mu}}$

———— 0
— — — .03
—·—·— .05

M = 0

M = 0.70

M = 0.50

Ejector pressure ratio, $p_{t,s}/p_{t,p}$

Jet total-pressure ratio, $p_{t,p}/p_\infty$

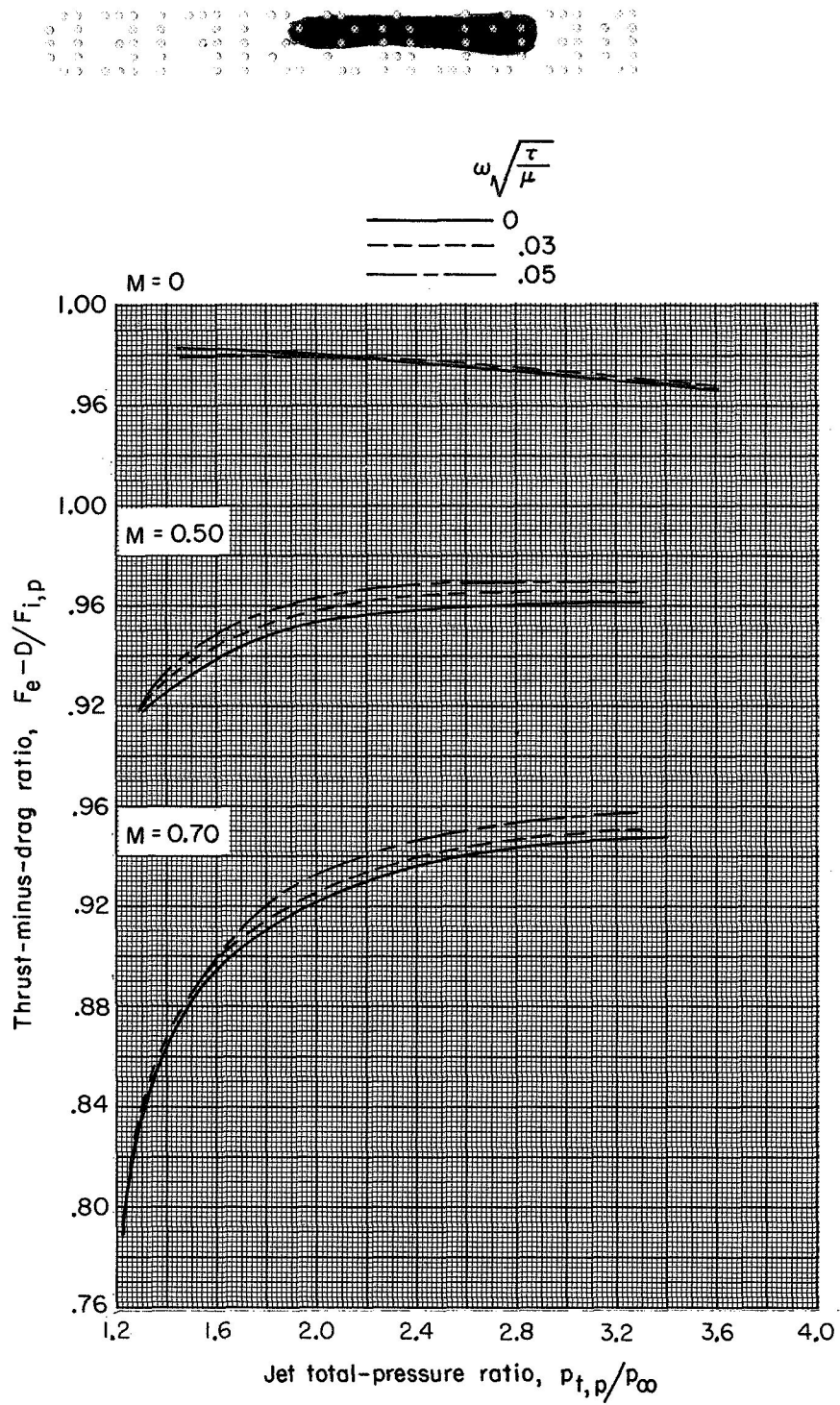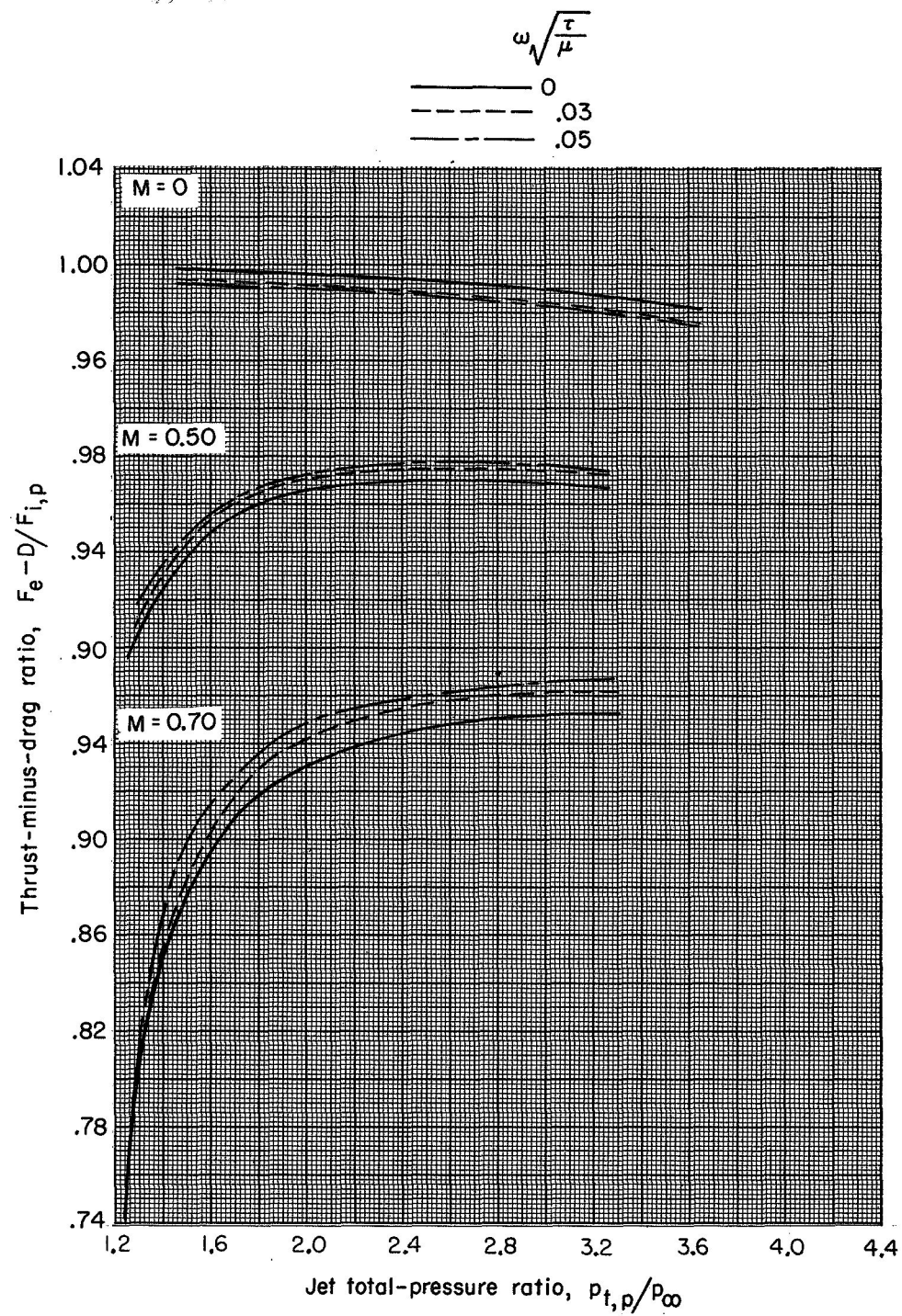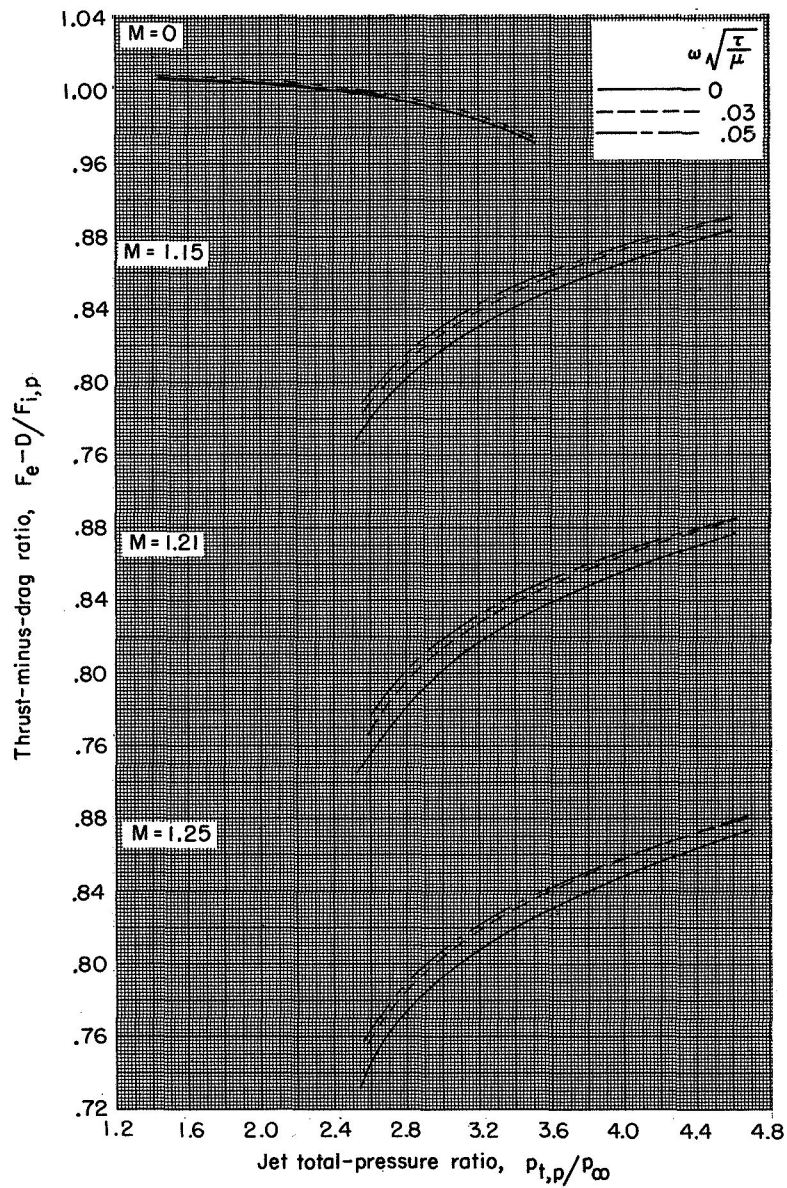Jet total-pressure ratio, $p_{t,p}/p_\infty$

(d) Configuration M-31.
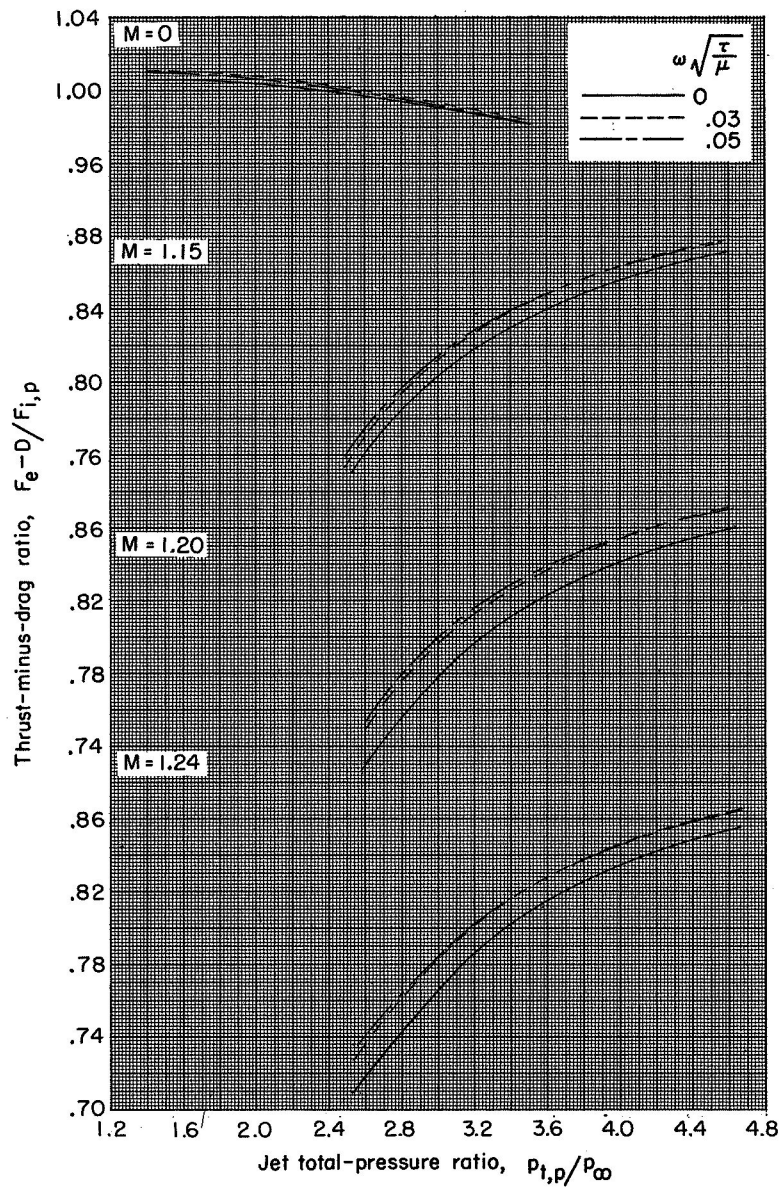
Figure 7.- Continued.
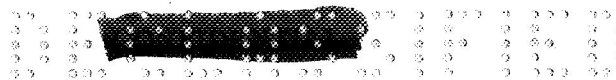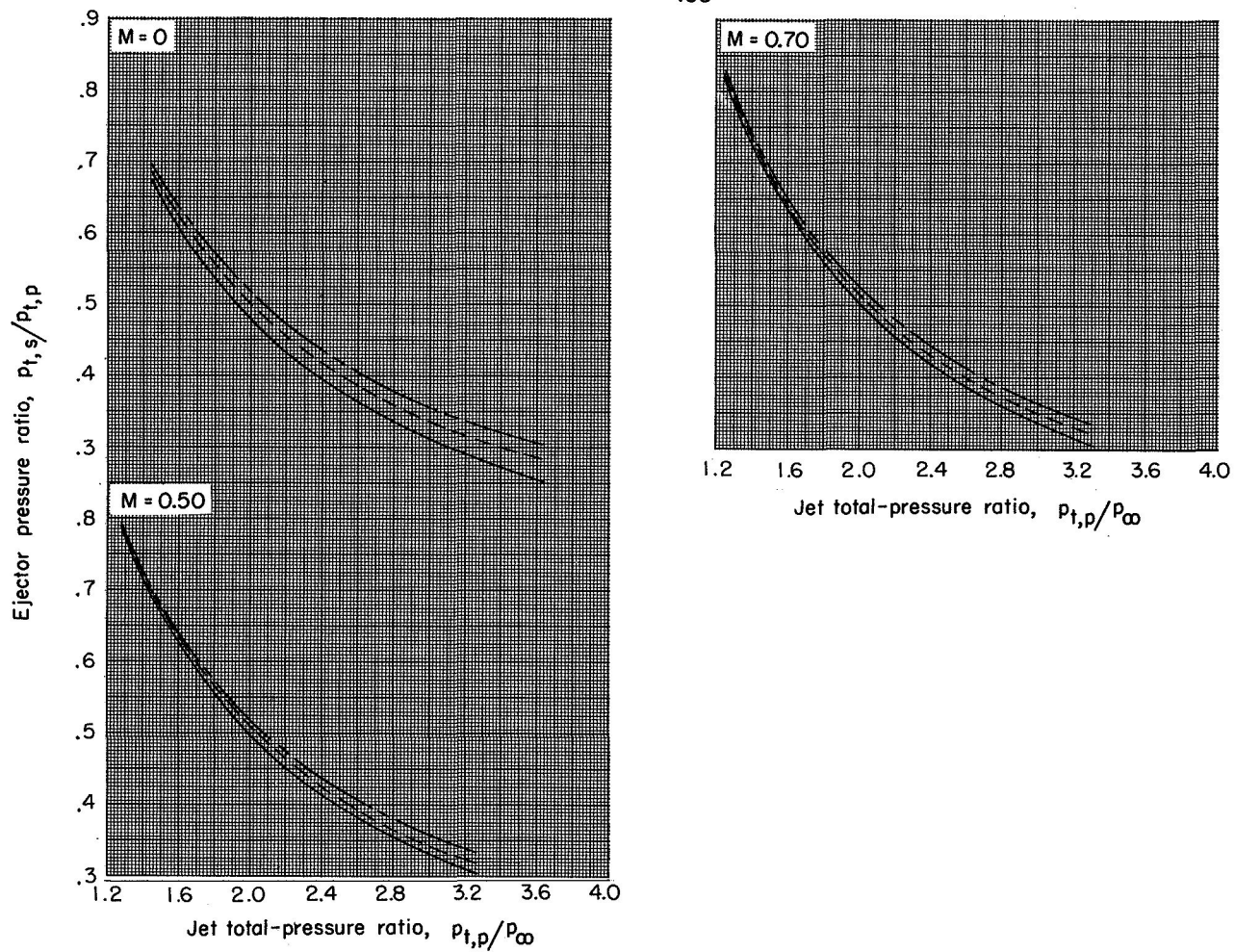
(e) Configuration M-23.

Figure 7.- Continued.
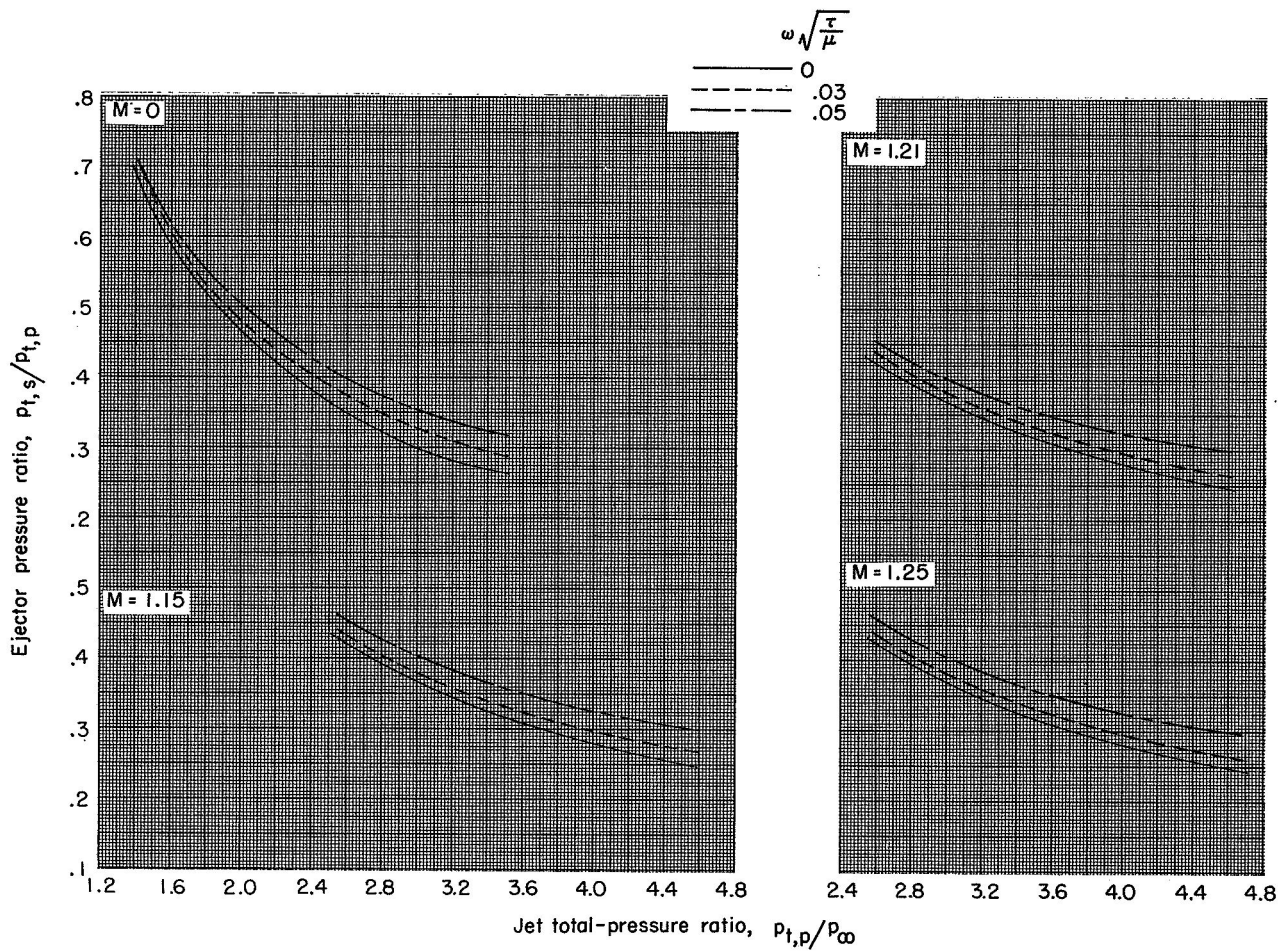
(f) Configuration A-11.

Figure 7.- Continued.

(g) Configuration A-13.

Figure 7.- Continued.

(h) Configuration A-21.

Figure 7.- Continued.

(i) Configuration A-31.

Figure 7.- Continued.

(j) Configuration A-23.

Figure 7.- Concluded.

(a) Configuration M-11.

Figure 8.- Variation of gross ejector thrust-minus-drag ratio with primary total-pressure ratio for constant corrected weight-flow ratios and Mach numbers.
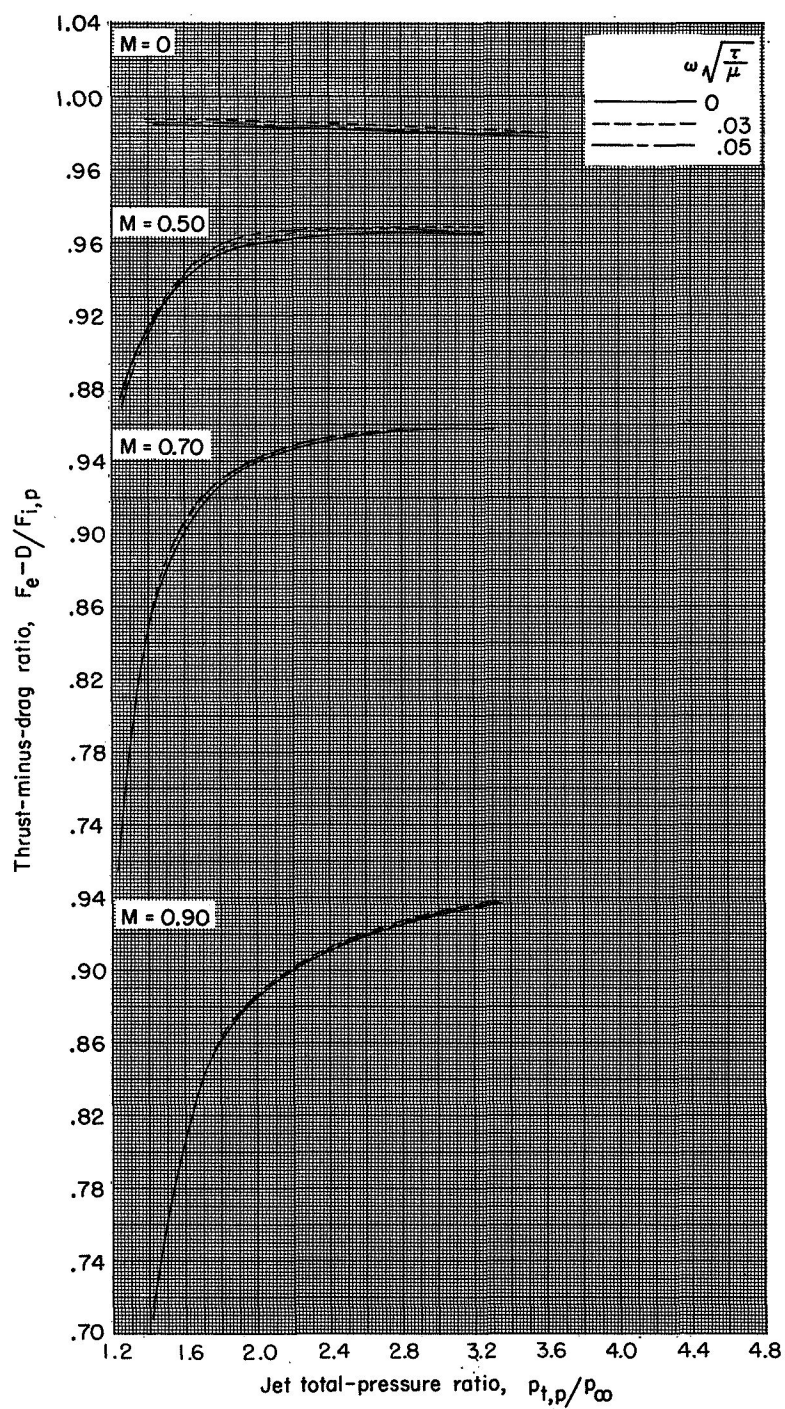
(b) Configuration M-13.

Figure 8.- Continued.

$$\omega\sqrt{\frac{\tau}{\mu}}$$

————	0
— — — —	.03
—·—·—	.05

Jet total-pressure ratio, $p_{t,p}/p_\infty$

(c) Configuration M-21.

Figure 8.- Continued.

49

(d) Configuration M-31.

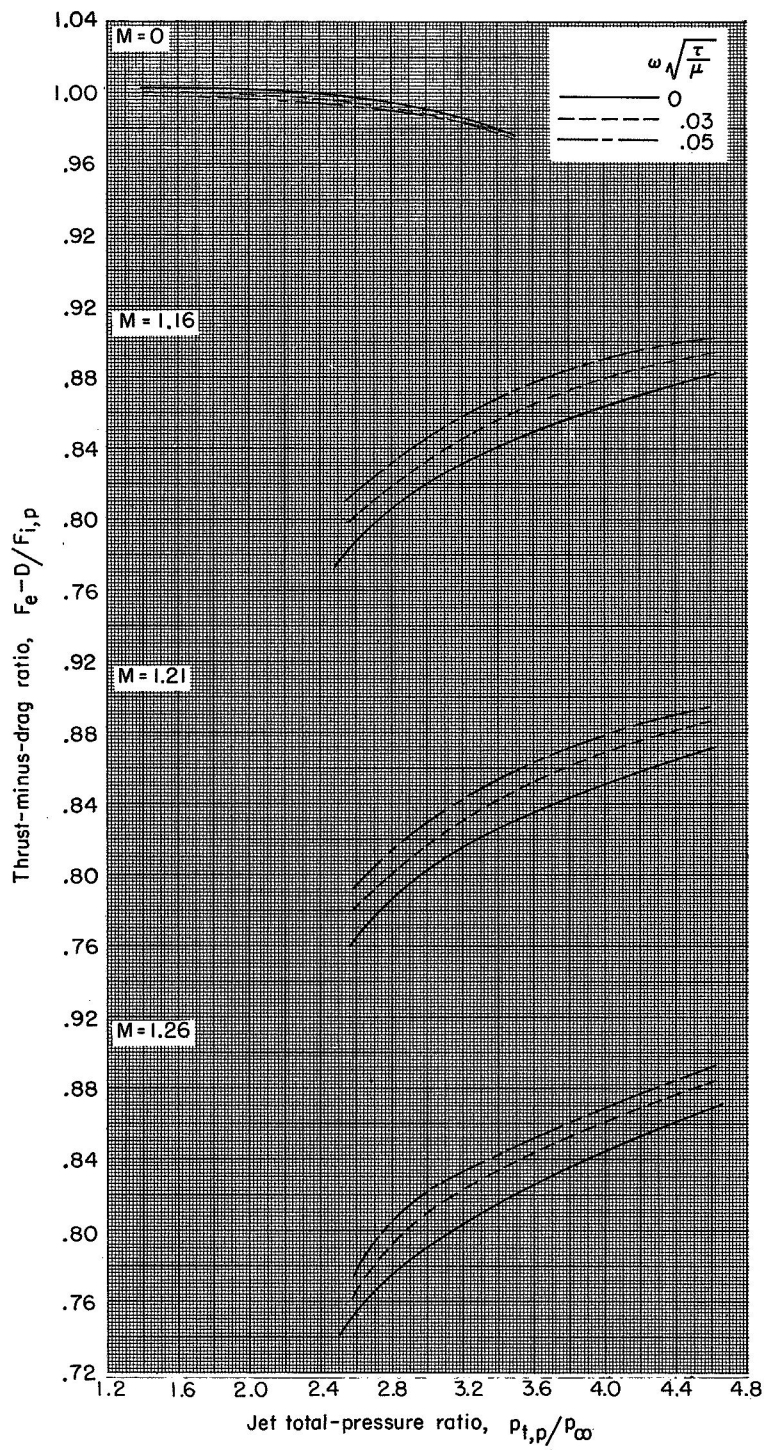Figure 8.- Continued.

(e) Configuration M-23.

Figure 8.- Continued.

(f) Configuration A-11.

Figure 8.- Continued.

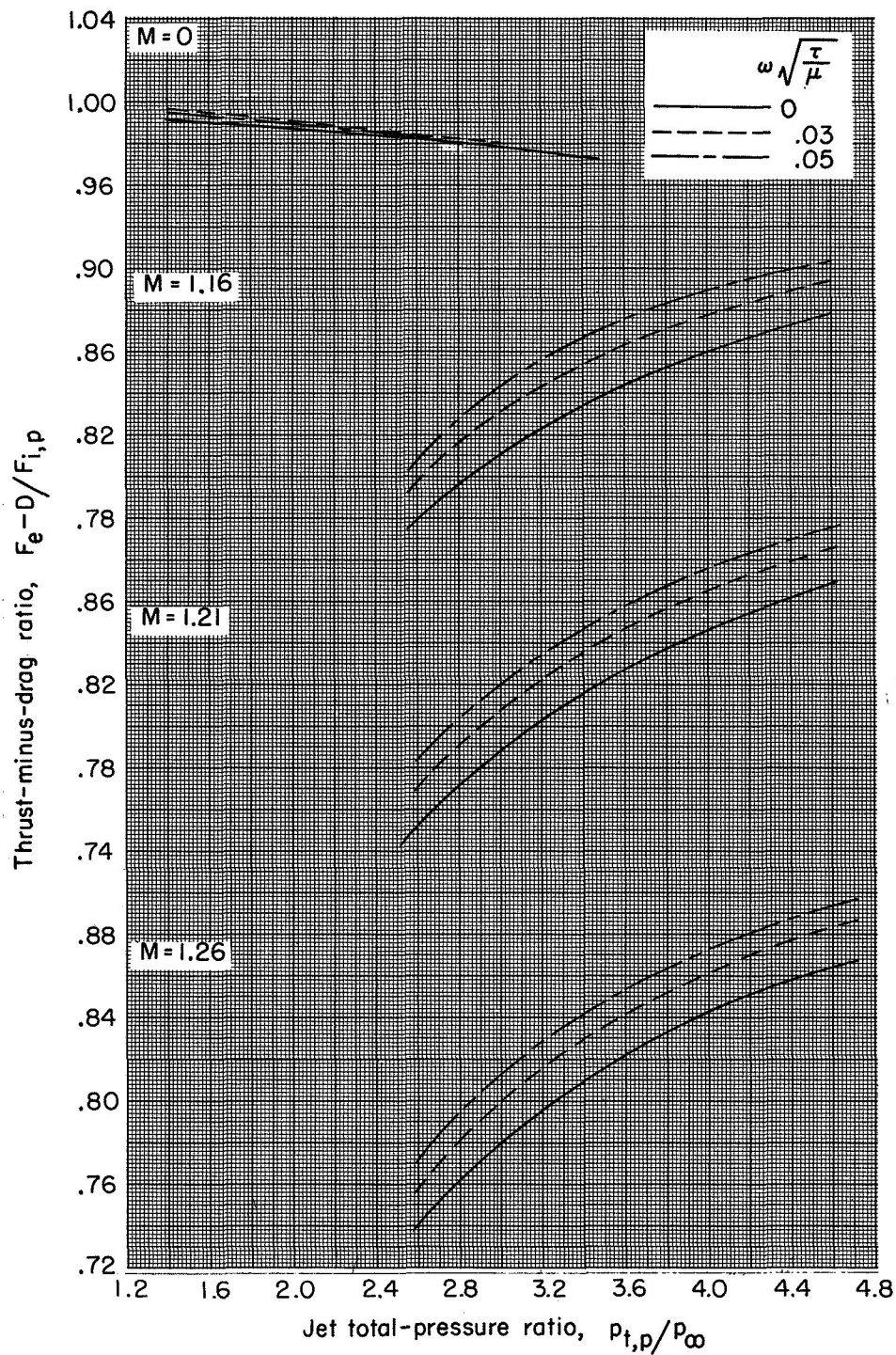(g) Configuration A-13.

Figure 8.- Continued.

Jet total-pressure ratio, $P_{t,p}/P_\infty$

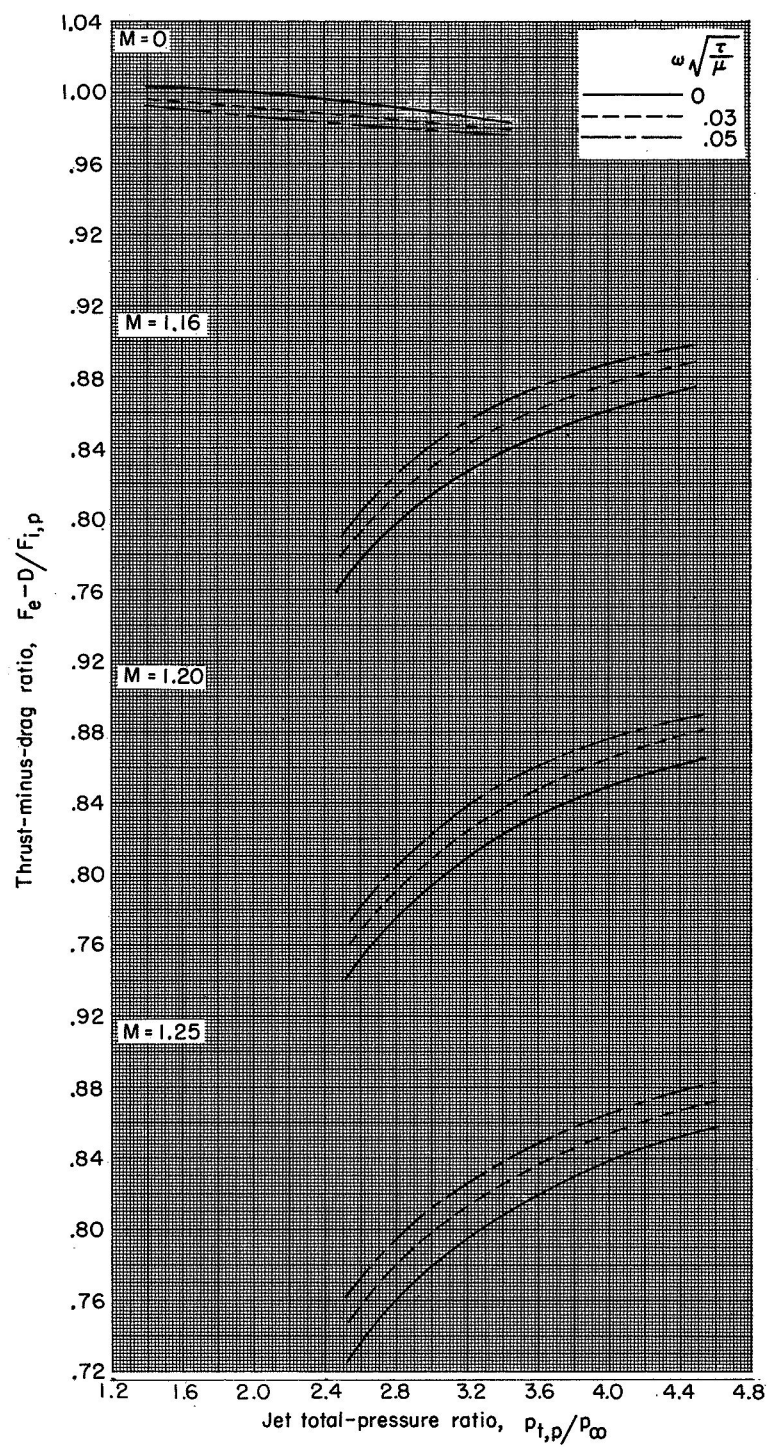Thrust-minus-drag ratio, $F_e-D/F_{i,p}$

(h) Configuration A-21.

Figure 8.- Continued.

(i) Configuration A-31.

Figure 8.- Continued.

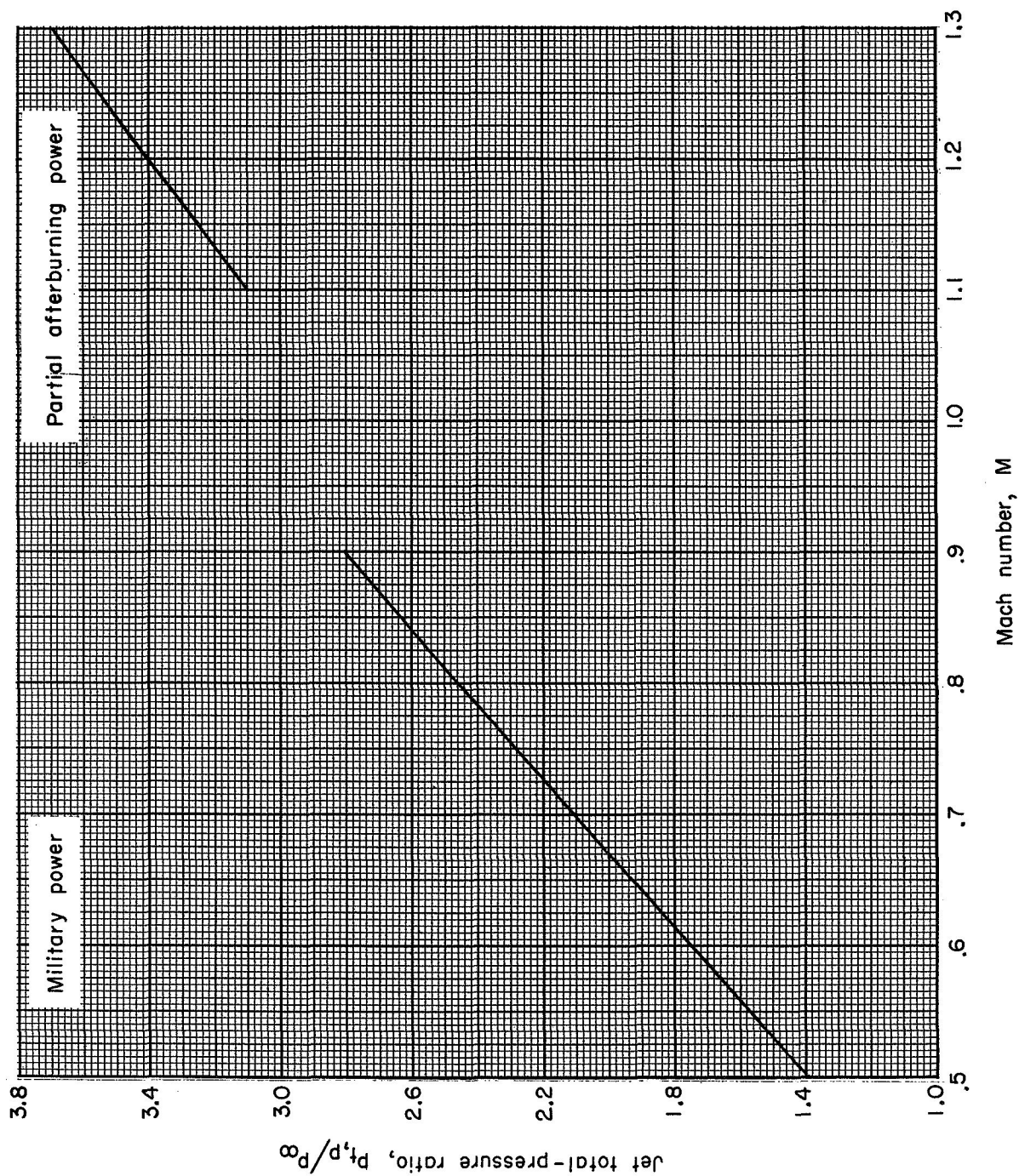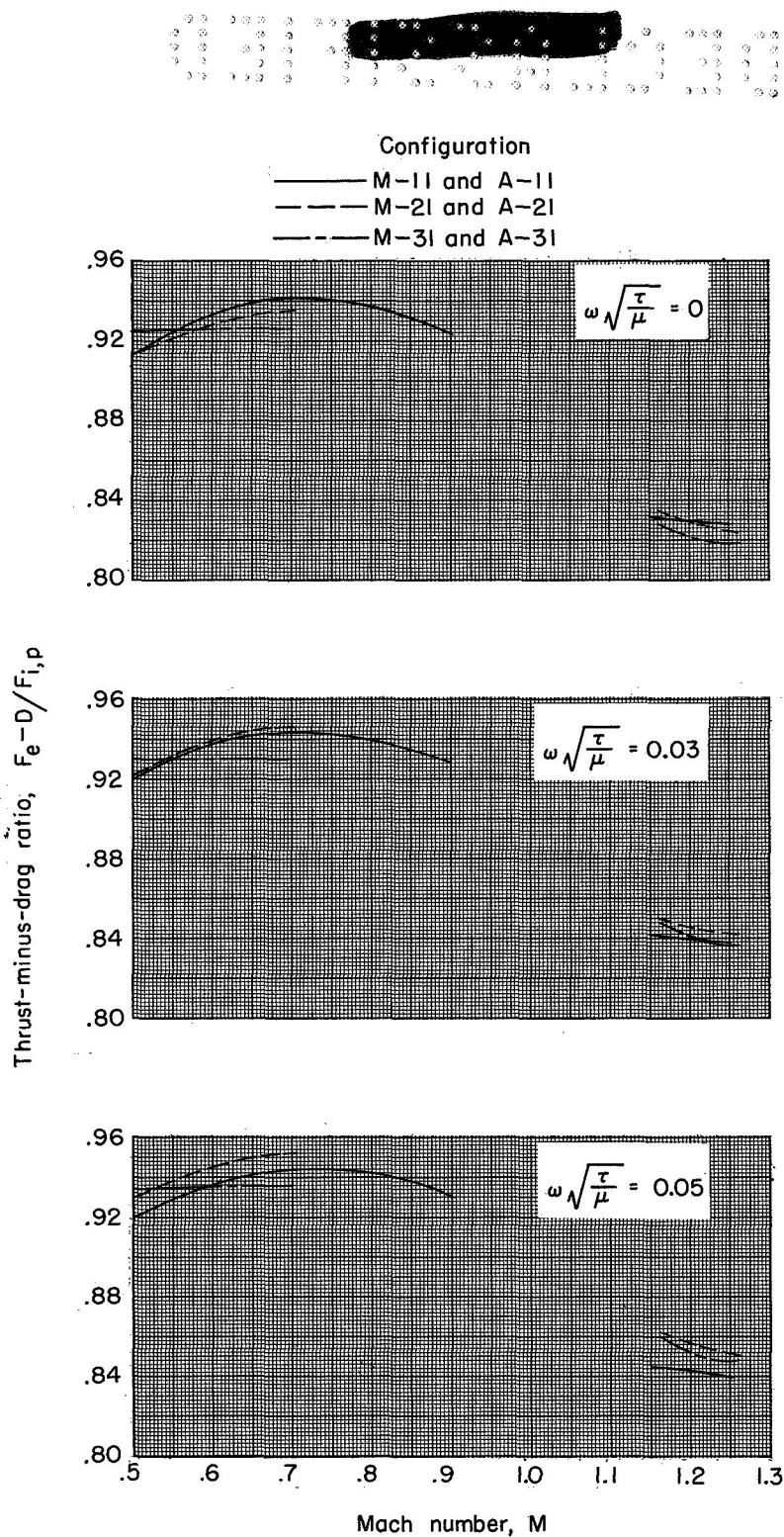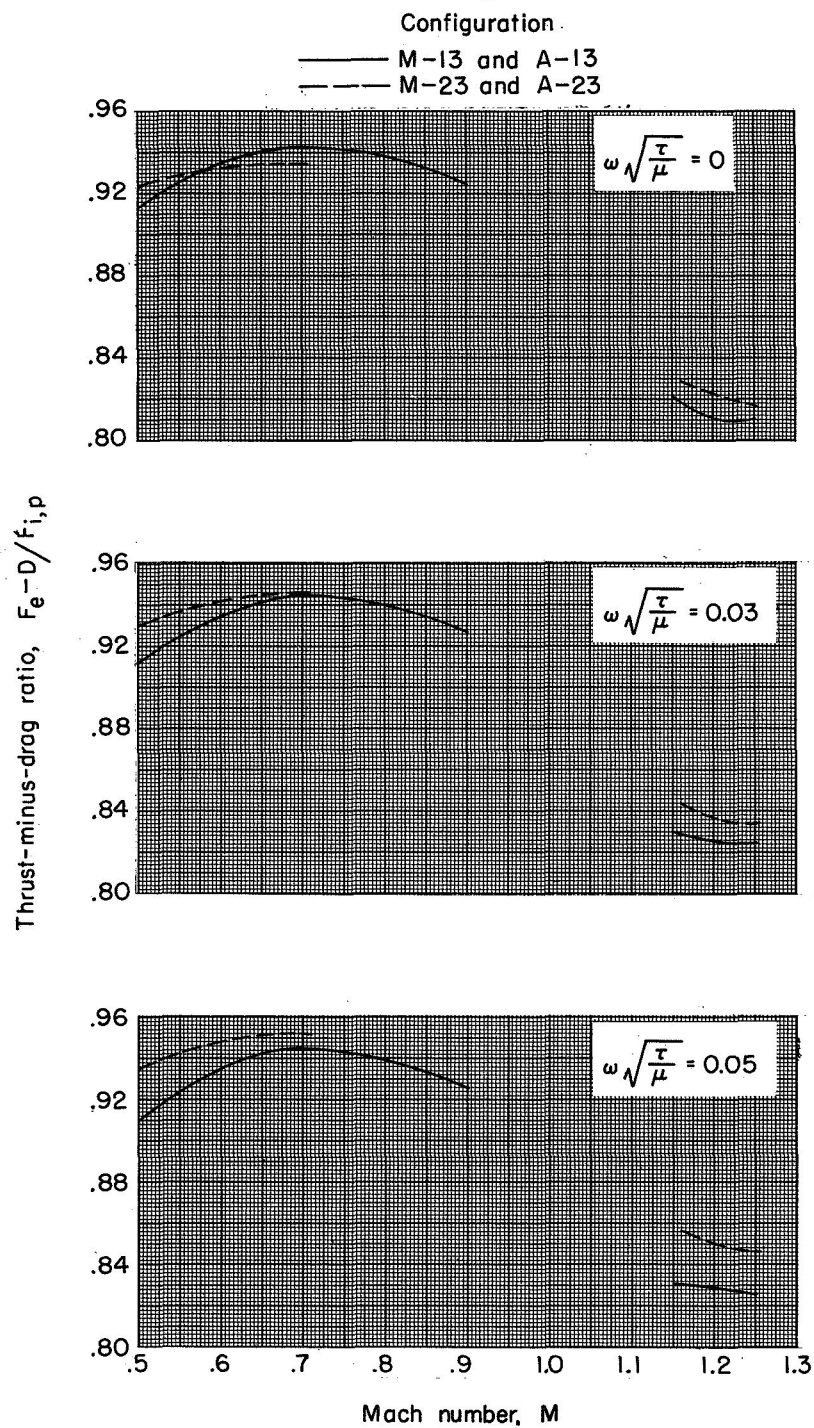(j) Configuration A-23.

Figure 8.- Concluded.

Figure 9.- Primary-jet total-pressure ratio as a function of Mach number for a typical turbofan engine.

(a) Fixed-open, free-floating, and partially blocked blow-in-door configurations; all with conical shroud.

Figure 10.- Gross ejector thrust-minus-drag ratio as a function of Mach number at design pressure ratio for constant corrected weight-flow ratios.

Configuration
————— M-13 and A-13
— — — M-23 and A-23

Thrust-minus-drag ratio, $F_e - D/F_{i,p}$

$\omega \sqrt{\dfrac{\tau}{\mu}} = 0$

$\omega \sqrt{\dfrac{\tau}{\mu}} = 0.03$

$\omega \sqrt{\dfrac{\tau}{\mu}} = 0.05$

Mach number, M

(b) Fixed-open and free-floating blow-in-door configurations; both with curved shroud.
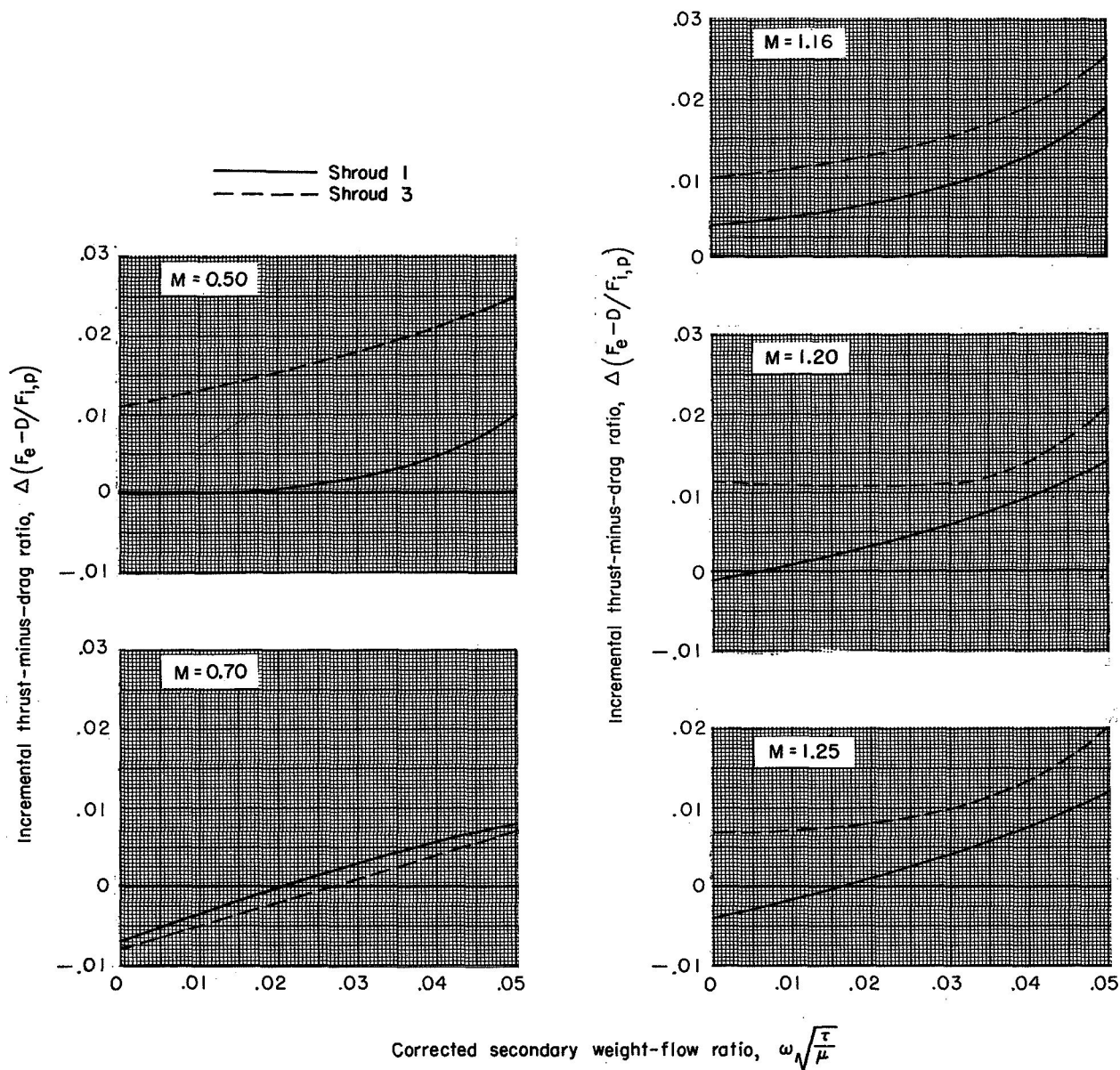
Figure 10.- Concluded.

Figure 11.- Change in gross ejector thrust-minus-drag performance ratio between free-floating and fixed-open blow-in-door nozzle configurations as a function of corrected secondary weight-flow ratio for schedule total-pressure ratios.

"The aeronautical and space activities of the United States shall be conducted so as to contribute . . . to the expansion of human knowledge of phenomena in the atmosphere and space. The Administration shall provide for the widest practicable and appropriate dissemination of information concerning its activities and the results thereof."

—NATIONAL AERONAUTICS AND SPACE ACT OF 1958

NASA SCIENTIFIC AND TECHNICAL PUBLICATIONS

TECHNICAL REPORTS: Scientific and technical information considered important, complete, and a lasting contribution to existing knowledge.

TECHNICAL NOTES: Information less broad in scope but nevertheless of importance as a contribution to existing knowledge.

TECHNICAL MEMORANDUMS: Information receiving limited distribution because of preliminary data, security classification, or other reasons.

CONTRACTOR REPORTS: Scientific and technical information generated under a NASA contract or grant and considered an important contribution to existing knowledge.

TECHNICAL TRANSLATIONS: Information published in a foreign language considered to merit NASA distribution in English.

SPECIAL PUBLICATIONS: Information derived from or of value to NASA activities. Publications include conference proceedings, monographs, data compilations, handbooks, sourcebooks, and special bibliographies.

TECHNOLOGY UTILIZATION PUBLICATIONS: Information on technology used by NASA that may be of particular interest in commercial and other non-aerospace applications. Publications include Tech Briefs, Technology Utilization Reports and Notes, and Technology Surveys.

Details on the availability of these publications may be obtained from:

SCIENTIFIC AND TECHNICAL INFORMATION DIVISION
NATIONAL AERONAUTICS AND SPACE ADMINISTRATION
Washington, D.C. 20546